not detect any types of Nedd8 derivatives in LC–MS/MS analysis, the Western blotting analysis of immunoaffinity-purified complexes with the Nedd8 specific antibody revealed several bands (Fig. 1D). The predicted molecular size of these bands indicates that UCH-L1 may interact with mono-Nedd8 while UCH-L3 may interact with di-Nedd8. UCHs are reported to show only weak affinity for Nedd8 compared with Ub. In addition, the expression level of Nedd8 protein is presumably low compared with that of Ub. These two differences might account for the limited amount of Nedd8 derivatives in the immunoaffinity-purified complex that can only be detected by Western blotting analysis. These interactions need to be further analyzed.

In conclusion, our analyses indicate that the major interacting partner of UCH-L1 is mono-Ub while that of UCH-L3 is di-Ub. These interactions appear to be responsible for the inhibition of deubiquitinating activity.

Acknowledgements

This work was supported by grants-in-aid for scientific research from the Japan Society for the Promotion of Science; a research grant in priority area research from the Ministry of Education, Culture, Sports, Science, and Technology, Japan; grants-in-aid for scientific research from the Ministry of Health, Labor, and Welfare, Japan; and the Program for Promotion of Fundamental Studies in Health Sciences of the National Institute of Biomedical Innovation and the New Energy and Industrial Technology Development Organization, Japan.

The authors thank Yoshihiro Nakatani and Hidesato Ogawa for providing the retroviral expression system and immunoaffinity purification system; Hiromi Fujita for the care and breeding of animals; Mari Suzuki, Yukihiro Tsuchiya, Tomohiro Kabuta and Yasuyuki Suzuki for valuable discussions.

References

Das, C., Hoang, Q.Q., Kreinbring, C.A., Luchansky, S.J., Meray, R.K., Ray, S.S., Lansbury, P.T., Ringe, D., Petsko, G.A., 2006. Structural basis for conformational plasticity of the Parkinson's disease-associated ubiquitin hydrolase UCH-L1. Proc. Natl. Acad. Sci. U. S. A. 103, 4675–4680.

Glickman, M.H., Ciechanover, A., 2002. The ubiquitin-proteasome proteolytic pathway: destruction for the sake of construction. Physiol. Rev. 82, 373–428.

Harada, T., Harada, C., Wang, Y.L., Osaka, H., Amanai, K., Tanaka, K., Takizawa, S., Setsuie, R., Sakurai, M., Sato, Y., Noda, M., Wada, K., 2004. Role of ubiquitin carboxy terminal hydrolase-L1 in neural cell apoptosis induced by ischemic retinal injury in vivo. Am. J. Pathol. 164, 59–64.

Hegde, A., Upadhya, S., 2007. The ubiquitin–proteasome pathway in health and disease of the nervous system. Trends Neurosci. 30, 587–595.

Hemelaar, J., Borodovsky, A., Kessler, B.M., Reverter, D., Cook, J., Kolli, N., Gan-Erdene, T., Wilkinson, K.D., Gill, G., Lima, C.D., Ploegh, H.L., Ovaa, H., 2004. Specific and covalent targeting of conjugating and deconjugating enzymes of ubiquitin-like proteins. Mol. Cell Biol. 24, 84–95.

Hershko, A., Ciechanover, A., 1998. The ubiquitin system. Annu. Rev. Biochem. 67, 425–479.

Hicke, L., 2001. Protein regulation by monoubiquitin. Nat. Rev. Mol. Cell Biol. 2, 195–201.

Hochstrasser, M., 2006. Lingering mysteries of ubiquitin-chain assembly. Cell 124, 27–34.

Johnston, S.C., Larsen, C.N., Cook, W.J., Wilkinson, K.D., Hill, C.P., 1997. Crystal structure of a deubiquitinating enzyme (human UCH-L3) at 1,8 A resolution. Embo J. 16, 3787–3796.

Kabuta, T., Setsuie, R., Mitsui, T., Kinugawa, A., Sakurai, M., Aoki, S., Uchida, K., Wada, K., 2008. Aberrant molecular properties shared by familial Parkinson's disease-associated mutant UCH-L1 and carbonyl-modified UCH-L1. Hum. Mol. Genet. 17, 1482–1496.

Kirisako, T., Kamei, K., Murata, S., Kato, M., Fukumoto, H., Kanie, M., Sano, S., Tokunaga, F., Tanaka, K., Iwai, K., 2006. A ubiquitin ligase complex assembles linear polyubiquitin chains. Embo J. 25, 4877–4887.

Kirkpatrick, D., Denison, C., Gygi, S., 2005. Weighing in on ubiquitin: the expanding role of mass-spectrometry-based proteomics. Nat. Cell Biol. 7, 750–757.

Kurihara, L.J., Kikuchi, T., Wada, K., Tilghman, S.M., 2001. Loss of Uch-L1 and Uch-L3 leads to neurodegeneration, posterior paralysis and dysphagia. Hum. Mol. Genet. 10, 1963–1970.

Kurihara, L.J., Semenova, E., Levorse, J.M., Tilghman, S.M., 2000. Expression and functional analysis of Uch-L3 during mouse development. Mol. Cell Biol. 20, 2498–2504.

Kwon, J., Wang, Y.L., Setsuie, R., Sekiguchi, S., Sakurai, M., Sato, Y., Lee, W.W., Ishii, Y., Kyuwa, S., Noda, M., Wada, K., Yoshikawa, Y., 2004. Developmental regulation of ubiquitin C-terminal hydrolase isozyme expression during spermatogenesis in mice. Biol. Reprod. 71, 515–521.

Larsen, C.N., Krantz, B.A., Wilkinson, K.D., 1998. Substrate specificity of deubiquitinating enzymes: ubiquitin C-terminal hydrolases. Biochemistry 37, 3358–3368.

Larsen, C.N., Price, J.S., Wilkinson, K.D., 1996. Substrate binding and catalysis by ubiquitin C-terminal hydrolases: identification of two active site residues. Biochemistry 35, 6735–6744.

Leroy, E., Boyer, R., Auburger, G., Leube, B., Ulm, G., Mezey, E., Harta, G., Brownstein, M.J., Jonnalagada, S., Chernova, T., Dehejia, A., Lavedan, C., Gasser, T., Steinbach, P.J., Wilkinson, K.D., Polymeropoulos, M.H., 1998. The ubiquitin pathway in Parkinson's disease. Nature 395, 451–452.

Liu, Y., Fallon, L., Lashuel, H.A., Liu, Z., Lansbury Jr., P.T., 2002. The UCH-L1 gene encodes two opposing enzymatic activities that affect alpha-synuclein degradation and Parkinson's disease susceptibility. Cell 111, 209–218.

Manago, Y., Kanahori, Y., Shimada, A., Sato, A., Amano, T., Sato-Sano, Y., Setsuie, R., Sakurai, M., Aoki, S., Wang, Y.L., Osaka, H., Wada, K., Noda, M., 2005. Potentiation of ATP-induced currents due to the activation of P2X receptors by ubiquitin carboxy-terminal hydrolase L1. J. Neurochem. 92, 1061–1072.

Misaghi, S., Galardy, P.J., Meester, W.J., Ovaa, H., Ploegh, H.L., Gaudet, R., 2005. Structure of the ubiquitin hydrolase UCH-L3 complexed with a suicide substrate. J. Biol. Chem. 280, 1512–1520.

Mukhopadhyay, D., Riezman, H., 2007. Proteasome-independent functions of ubiquitin in endocytosis and signaling. Science 315, 201–205.

Nijman, S.M., Luna-Vargas, M.P., Velds, A., Brummelkamp, T.R., Dirac, A.M., Sixma, T.K., Bernards, R., 2005. A genomic and functional inventory of deubiquitinating enzymes. Cell 123, 773–786.

Nishikawa, K., Li, H., Kawamura, R., Osaka, H., Wang, Y.L., Hara, Y., Hirokawa, T., Manago, Y., Amano, T., Noda, M., Aoki, S., Wada, K., 2003. Alterations of structure and hydrolase activity of parkinsonism-associated human ubiquitin carboxyl-terminal hydrolase L1 variants. Biochem. Biophys. Res. Commun. 304, 176–183.

Ogawa, H., Ishiguro, K., Gaubatz, S., Livingston, D.M., Nakatani, Y., 2002. A complex with chromatin modifiers that occupies E2F- and Myc-responsive genes in G0 cells. Science 296, 1132–1136.

Osaka, H., Wang, Y.L., Takada, K., Takizawa, S., Setsuie, R., Li, H., Sato, Y., Nishikawa, K., Sun, Y.J., Sakurai, M., Harada, T., Hara, Y., Kimura, I., Chiba, S., Namikawa, K., Kiyama, H., Noda, M., Aoki, S., Wada, K., 2003. Ubiquitin carboxy-terminal hydrolase L1 binds to and stabilizes monoubiquitin in neuron. Hum. Mol. Genet. 12, 1945–1958.

Rubinsztein, D.C., 2006. The roles of intracellular protein-degradation pathways in neurodegeneration. Nature 443, 780–786.

Saigoh, K., Wang, Y.L., Suh, J.G., Yamanishi, T., Sakai, Y., Kiyosawa, H., Harada, T., Ichihara, N., Wakana, S., Kikuchi, T., Wada, K., 1999. Intragenic deletion in the gene encoding ubiquitin carboxy-terminal hydrolase in gad mice. Nat. Genet. 23, 47–51.

Sakurai, M., Ayukawa, K., Setsuie, R., Nishikawa, K., Hara, Y., Ohashi, H., Nishimoto, M., Abe, T., Kudo, Y., Sekiguchi, M., Sato, Y., Aoki, S., Noda, M., Wada, K., 2006. Ubiquitin C-terminal hydrolase L1 regulates the morphology of neural progenitor cells and modulates their differentiation. J. Cell Sci. 119, 162–171.

Sakurai, M., Sekiguchi, M., Zushida, K., Yamada, K., Nagamine, S., Kabuta, T., Wada, K., 2008. Reduction in memory in passive avoidance learning, exploratory behaviour and synaptic plasticity in mice with a spontaneous deletion in the ubiquitin C-terminal hydrolase L1 gene. Eur. J. Neurosci. 27, 691–701.

Sano, Y., Furuta, A., Setsuie, R., Kikuchi, H., Wang, Y.L., Sakurai, M., Kwon, J., Noda, M., Wada, K., 2006. Photoreceptor cell apoptosis in the retinal degeneration of Uchl3-deficient mice. Am. J. Pathol. 169, 132–141.

Semenova, E., Wang, X., Jablonski, M.M., Levorse, J., Tilghman, S.M., 2003. An engineered 800 kilobase deletion of Uchl3 and Lmo7 on mouse chromosome 14 causes defects in viability, postnatal growth and degeneration of muscle and retina. Hum. Mol. Genet. 12, 1301–1312.

Setsuie, R., Wada, K., 2007. The functions of UCH-L1 and its relation to neurodegenerative diseases. Neurochem. Int. 51, 105–111.

Setsuie, R., Wang, Y.L., Mochizuki, H., Osaka, H., Hayakawa, H., Ichihara, N., Li, H., Furuta, A., Sano, Y., Sun, Y.J., Kwon, J., Kabuta, T., Yoshimi, K., Aoki, S., Mizuno, Y., Noda, M., Wada, K., 2007. Dopaminergic neuronal loss in transgenic mice expressing the Parkinson's disease-associated UCH-L1 I93M mutant. Neurochem. Int. 50, 119–129.

Todaro, G.J., Green, H., 1963. Quantitative studies of the growth of mouse embryo cells in culture and their development into established lines. J. Cell. Biol. 17, 299–313.

van Nocker, S., Vierstra, R.D., 1993. Multiubiquitin chains linked through lysine 48 are abundant in vivo and are competent intermediates in the ubiquitin proteolytic pathway. J. Biol. Chem. 268, 24766–24773.

Wada, H., Kito, K., Caskey, L.S., Yeh, E.T., Kamitani, T., 1998. Cleavage of the C-terminus of NEDD8 by UCH-L3. Biochem. Biophys. Res. Commun. 251, 688–692.

Walters, B., Campbell, S., Chen, P., Taylor, A., Schroeder, D., Dobrunz, L., Artavanistsakonas, K., Ploegh, H., Wilson, J., Cox, G., 2008. Differential effects of Usp14

and Uch-L1 on the ubiquitin proteasome system and synaptic activity. Mol. Cell. Neurosci. 45.
Wilkinson, K.D., 1997. Regulation of ubiquitin-dependent processes by deubiquitinating enzymes. Faseb J. 11, 1245–1256.
Wilkinson, K.D., Laleli-Sahin, E., Urbauer, J., Larsen, C.N., Shih, G.H., Haas, A.L., Walsh, S.T., Wand, A.J., 1999. The binding site for UCH-L3 on ubiquitin: mutagenesis and NMR studies on the complex between ubiquitin and UCH-L3. J. Mol. Biol. 291, 1067–1077.
Wilkinson, K.D., Lee, K.M., Deshpande, S., Duerksen-Hughes, P., Boss, J.M., Pohl, J., 1989. The neuron-specific protein PGP 9.5 is a ubiquitin carboxyl-terminal hydrolase. Science 246, 670–673.
Wood, M., Kaplan, M., Brensinger, C., Guo, W., Abel, T., 2005. Ubiquitin C-terminal hydrolase L3 (Uchl3) is involved in working memory. Hippocampus 15, 610–621.
Yin, L., Krantz, B., Russell, N.S., Deshpande, S., Wilkinson, K.D., 2000. Nonhydrolyzable diubiquitin analogues are inhibitors of ubiquitin conjugation and deconjugation. Biochemistry 39, 10001–10010.

Journal of Neurochemistry JNC

JOURNAL OF NEUROCHEMISTRY | 2009 | 108 | 932–944 doi: 10.1111/j.1471-4159.2008.05827.x

Effects of UCH-L1 on α-synuclein over-expression mouse model of Parkinson's disease

Toru Yasuda,* Tomoko Nihira,* Yong-Ri Ren,* Xu-Qing Cao,† Keiichiro Wada,† Rieko Setsuie,‡ Tomohiro Kabuta,‡ Keiji Wada,‡ Nobutaka Hattori,† Yoshikuni Mizuno* and Hideki Mochizuki*,†

*Research Institute for Diseases of Old Age, Juntendo University, Tokyo, Japan

†Department of Neurology, Juntendo University School of Medicine, Tokyo, Japan

‡Department of Degenerative Neurological Diseases, National Institute of Neuroscience, National Center of Neurology and Psychiatry, Tokyo, Japan

Abstract

The rare inherited form of Parkinson's disease (PD), *PARK5*, is caused by a missense mutation in *ubiquitin carboxy-terminal hydrolase-L1* (*UCH-L1*) gene, resulting in Ile93Met substitution in its gene product (UCH-L1^{Ile93Met}). *PARK5* is inherited in an autosomal-dominant mode, but whether the Ile93Met mutation gives rise to a gain-of-toxic-function or loss-of-function of UCH-L1 protein remains controversial. Here, we investigated the selective vulnerabilities of dopaminergic (DA) neurons in UCH-L1-transgenic (Tg) and spontaneous UCH-L1-null *gracile axonal dystrophy* mice to an important PD-causing insult, abnormal accumulation of α-synuclein (αSyn). Immunohistochemistry of midbrain sections of a patient with sporadic PD showed αSyn- and UCH-L1-double-positive Lewy bodies in nigral DA neurons, suggesting physical and/or functional interaction between the two proteins in human PD brain. Recombinant adeno-associated viral vector-mediated over-expression of αSyn for 4 weeks significantly enhanced the loss of nigral DA cell bodies in UCH-L1^{Ile93Met}-Tg mice, but had weak effects in age-matched UCH-L1$^{wild\text{-}type}$-Tg mice and non-Tg littermates. In contrast, the extent of αSyn-induced DA cell loss in *gracile axonal dystrophy* mice was not significantly different from wild-type littermates at 13-weeks post-injection. Our results support the hypothesis that *PARK5* is caused by a gain-of-toxic-function of UCH-L1^{Ile93Met} mutant, and suggest that regulation of UCH-L1 in nigral DA cells could be a future target for treatment of PD.

Keywords: α-synuclein, adeno-associated virus, dopaminergic neurons, Parkinson's disease, ubiquitin carboxy-terminal hydrolase-L1.

J. Neurochem. (2009) **108**, 932–944.

Parkinson's disease (PD) is a progressive neurodegenerative disorder characterized clinically by resting tremor, rigidity, akinesia, and postural instability (Farrer 2006). The major pathological hallmarks of PD are the selective loss of nigrostriatal dopaminergic (DA) neurons and the presence of intraneuronal protein inclusions termed Lewy bodies, in the surviving DA neurons. Sporadic cases represent more than 90% of total patients with PD, while there exist several inherited forms (familial PD; fPD) caused by mutations in single genes. Identification and characterization of these causative genes and their products can help us understand the molecular mechanism(s) of DA neurodegeneration in the sporadic form of PD. Seven causative genes for fPDs have been identified to date; those encoding α-synuclein (αSyn), parkin, UCH-L1, PINK1, DJ-1, LRRK2, or ATP13A2 (Farrer 2006; Ramirez *et al.* 2006).

α-Synuclein is a pre-synaptic protein potentially involved in learning, synaptic plasticity, vesicle dynamics, and dopamine synthesis (Farrer 2006). The fPD *PARK1* is caused by

Received August 26, 2008; revised manuscript received November 6, 2008; accepted November 27, 2008.

Address correspondence and reprint requests to Hideki Mochizuki, Department of Neurology, Juntendo University School of Medicine, 2-1-1 Hongo, Bunkyo-ku, Tokyo, 113-8421, Japan.
E-mail: hideki@med.juntendo.ac.jp

Abbreviations used: αSyn, α-synuclein; DA, dopaminergic; DOPAC, 2-(3,4-dihydroxyphenyl)acetic acid; fPD, familial Parkinson's disease; *gad, gracile axonal dystrophy*; hrGFP, humanized recombinant green fluorescent protein; HVA, homovanillic acid; PBS, phosphate-buffered saline; PD, Parkinson's disease; rAAV, recombinant adeno-associated virus; SN, substantia nigra; SNpc, substantia nigra pars compacta; Tg, transgenic; TH, tyrosine hydroxylase; UCH-L1, ubiquitin carboxy-terminal hydrolase-L1.

missense mutations resulting in amino acid substitutions in αSyn protein (Ala53Thr, Ala30Pro, or Glu46Lys) (Polymeropoulos *et al.* 1997; Kruger *et al.* 1998; Zarranz *et al.* 2004). Furthermore, *PARK4* is caused by duplication or triplication of *αSyn* gene (*SNCA*) locus (Singleton *et al.* 2003; Nishioka *et al.* 2006). In sporadic cases of PD, αSyn protein is the major component of Lewy bodies (Spillantini *et al.* 1997; Baba *et al.* 1998). These findings suggest an important role for αSyn protein accumulation in DA cells in the pathogenesis of PD. Previous studies also reported that over-expression of αSyn protein by using a recombinant adeno-associated viral (rAAV) or lentiviral vector caused DA neurodegeneration in rats and monkeys (Kirik *et al.* 2002, 2003; Lo Bianco *et al.* 2002; Yamada *et al.* 2004; Yasuda *et al.* 2007).

Ubiquitin carboxy-terminal hydrolase-L1 constitutes 1–2% of brain proteins and functions in the ubiquitin-proteasome system (Wilkinson *et al.* 1989; Larsen *et al.* 1996, 1998). The ubiquitin hydrolase activity of UCH-L1 is important to free reusable ubiquitin monomers. UCH-L1 protein is also known to bind to and stabilize monomeric ubiquitin molecule (Osaka *et al.* 2003). *PARK5* is caused by a missense mutation in *UCH-L1* gene resulting in Ile93Met substitution in UCH-L1 protein (UCH-L1^{Ile93Met}), and inherited in an autosomal-dominant mode (Leroy *et al.* 1998). The UCH-L1^{Ile93Met} mutant was initially shown to have decreased ubiquitin hydrolase activity (Leroy *et al.* 1998; Nishikawa *et al.* 2003). In sporadic PD cases, wild-type UCH-L1 protein is deposited in Lewy bodies (Lowe *et al.* 1990). These controversial findings initiated a debate on whether the Ile93Met mutation results in gain-of-toxic-function or loss-of-function of UCH-L1 protein. Recently, we established transgenic (Tg) mice that over-express UCH-L1^{Ile93Met} protein of human origin (Setsuie *et al.* 2007). These mice showed behavioral and pathological phenotypes of Parkinsonism at 20 weeks of age (Setsuie *et al.* 2007). On the other hand, the *gracile axonal dystrophy* (*gad*) mouse, which exhibits age-dependent sensory ataxic phenotype and motor paresis, has spontaneous intragenic deletion of mouse *Uchl1* gene and systemic lack of the UCH-L1 protein expression (Saigoh *et al.* 1999). The pathological characteristics of these mice are 'dying-back' axonal degeneration in sensory and motor nerve terminals (Oda *et al.* 1992; Miura *et al.* 1993). However, they do not seem to show any pathological changes in the nigrostriatal DA pathway, especially the loss of DA cell bodies in the substantia nigra (SN). To our knowledge, no investigator has examined the vulnerability of DA neurons in *gad* mice to PD-causing insults.

The aim of the present study was to determine the functional interaction between αSyn and UCH-L1 proteins *in vivo*. Specifically, we examined whether the DA neurotoxicity associated with accumulation of αSyn protein is influenced by UCH-L1 mutation or absence of normal UCH-L1 activities. Identification of such interaction could be useful in the design of novel gene therapies that target UCH-L1.

Materials and methods

Human brain tissue

Autopsied brain of a 69-year-old female PD patient was used in this study. The diagnosis of PD was confirmed at the Department of Neurology, Juntendo University School of Medicine. The study protocol was approved by the Human Ethics Review Committee of Juntendo University School of Medicine. The autopsied midbrain tissue was cut into blocks, immediately fixed in phosphate-buffered 4% formaldehyde for 2 days. Then the tissue blocks were immersed in phosphate-buffered saline (PBS) containing 30% sucrose until sinking. Coronal sections were cut at a thickness of 30 μm using a freezing microtome.

Mice

The Tg mice lines of UCH-L1^{Ile93Met} (line H-hI93M) and UCH-L1$^{wild\text{-}type}$ (line hWT) were generated as described previously using fertilized eggs of C57BL/6 mice (Setsuie *et al.* 2007). Male UCH-L1^{Ile93Met}-Tg mice were bred with female C57BL/6 mice (Charles River Laboratories, Kanagawa, Japan), to obtain Tg and non-Tg littermates. The latter were used in the experiment at the ages of 13 weeks (denoted as 3-month-old) and 52–57 weeks (12-month-old). Male UCH-L1$^{wild\text{-}type}$-Tg mice were bred with female C57BL/6 mice, and the obtained Tg mice were used in the experiment at the ages of 13 weeks (3-month-old) and 53–57 weeks (12-month-old). At 3 and 12 months of age, the number of DA cells in UCH-L1^{Ile93Met}-Tg mice was not significantly different from those of age-matched non-Tg littermates (Setsuie *et al.* 2007; and this study, data not shown). Male and female mice heterozygous for *gad* allele were bred, and the obtained *gad* and wild-type littermates were used in the experiments at the age of 13 weeks (3-month-old). The *gad* mice line had been backcrossed to C57BL/6 background for at least 15 generations. The experimental protocol was approved by the Ethics Review Committee for Animal Experimentation of Juntendo University School of Medicine, and all surgical operations were performed according to rules set forth by the Ethics Committee for the Use of Laboratory Animals at Juntendo University.

Preparation of rAAV vector

The plasmid pAAV-MCS (CMV promoter; Stratagene, La Jolla, CA, USA) carrying human *αSyn* cDNA (pAAV-MCS-αSyn) was constructed as reported previously (Yamada *et al.* 2004). High-titer serotype-1 rAAV (rAAV1) vector stocks were prepared as described previously (Yasuda *et al.* 2007). In brief, the plasmid pAAV-MCS-αSyn or pAAV-hrGFP (humanized recombinant green fluorescent protein; Stratagene) was co-transfected with plasmids pHelper and Pack2/1 (kindly provided by Dr. T. Shimada, Nippon Medical School, Tokyo, Japan) to HEK293 cells using a standard calcium phosphate method (Sambrook and Russell 2001). After 48 h, the cells were harvested and the crude rAAV1 vector solutions were obtained by repeated freeze/thaw cycles. After ammonium sulfate precipitation, the virus particles were dissolved in PBS and applied to OptiSeal centrifugation tube (Beckman Coulter, Inc., Fullerton,

CA, USA). After overlaying the OptiPrep solution (Axis-Shield PoC AS, Oslo, Norway), the tube was processed by GradientMaster (BioComp Instruments, Inc., New Brunswick, Canada) to prepare a gradient layer of OptiPrep. The tube was then ultracentrifuged at 20 000 *g* for 18.5 h. The fractions containing high-titer rAAV1 vectors were collected and used for the injection into mice. The number of rAAV1 genome copies was quantified by PCR within the CMV promoter region using primers 5′-GACGTCAATAATGACG-TATG-3′ and 5′-GGTAATAGCGATGACTAATACG-3′. The titer of rAAV1 vector to produce human αSyn (designated rAAV1-αSyn) was 6×10^{11} genomes/mL, and the titer of rAAV1 vector to produce hrGFP (rAAV1-hrGFP) was 6×10^{11} genomes/mL.

Stereotaxic injection of rAAV1 vectors

Mice were anesthetized with sodium pentobarbital (50 mg/kg body weight; intraperitoneally, i.p.) and positioned in a stereotaxic frame. The skull was exposed, and a small portion of the skull over the SN was removed unilaterally with a dental drill. Subsequently, rAAV1-αSyn or rAAV1-hrGFP was injected unilaterally into the SN (2 μL, 2.8 mm posterior and 1.3 mm lateral from the bregma, 4.4 mm below the dural surface, tooth bar = −2 mm) through a 5-μL Hamilton microsyringe.

The rAAV1-injected UCH-L1$^{\text{wild-type}}$-Tg, UCH-L1$^{\text{Ile93Met}}$-Tg mice, and non-Tg littermates were killed at 4-weeks post-injection, while the rAAV1-injected *gad* and wild-type littermates were killed at 4-, 8-, or 13-weeks post-injection. Mice were deeply anesthetized with sodium pentobarbital (250 mg/kg body weight; i.p.) and perfused transcardially with PBS. The brains were removed *en bloc* from the skull, and cut coronally along the anterior tangent to the median eminence. The striatal tissues were then dissected and immediately frozen on dry ice. The posterior parts of brain blocks including the entire rostrocaudal extent of the SN were fixed overnight in 4% paraformaldehyde in PBS, and immersed in PBS containing 30% sucrose until sinking. Coronal sections of the SN were cut serially at 20 μm thickness by a freezing microtome.

Antibodies and immunohistochemistry

The primary antibodies used in this study were as follows; mouse anti-human αSyn (clone LB509; diluted at 1 : 100; Zymed Laboratories Inc., South San Francisco, CA, USA), rabbit anti-UCH-L1 (1 : 1000; Ultraclone, Isle of Wight, UK), rabbit anti-hrGFP (1 : 500; Stratagene), sheep anti-tyrosine hydroxylase (TH) (1 : 5000; Calbiochem, San Diego, CA, USA), rabbit anti-dopamine transporter (DAT) (1 : 200; Chemicon International Inc., Temecula, CA, USA), and rabbit anti-active caspase-3 (1 : 500; BD Biosciences, San Jose, CA, USA) antibodies. The free-floating coronal sections of the human and mice brains were washed in a PBS medium containing 0.05% Triton X-100 (PBS-T), soaked with 10% Block Ace (Yukijirushi-Nyugyo Co., Sapporo, Japan) in PBS-T, and then incubated with the primary antibody dissolved in PBS-T containing 2% Block Ace at 4°C for 24–48 h. Subsequently, for fluorescent visualization of the antigens, the sections were incubated for 2 h in the same fresh medium containing the following secondary antibodies. For human brain sections, FITC-conjugated anti-mouse IgG and Cy3-conjugated anti-rabbit IgG antibodies (1 : 500; Jackson ImmunoResearch Laboratories, Inc., West Grove, PA, USA) were used. For mouse brain sections, FITC-conjugated anti-mouse IgG or anti-rabbit IgG antibody (1 : 500; Jackson ImmunoResearch Laboratories, Inc.) and Cy3-conjugated anti-sheep IgG antibody (1 : 500; Jackson ImmunoResearch Laboratories, Inc.) were used. Sections on the slides were mounted using Vectashield Mounting Medium with 4′,6-diamidino-2-phenylindole (DAPI) (Vector Laboratories Inc., Burlingame, CA, USA). Images were captured using a confocal laser-scanning microscope (LSM510, Zeiss, Jena, Germany). For colorimetric visualization of the antigen, the sections were incubated for 2 h in the same fresh medium containing biotinylated secondary antibody (anti-mouse, anti-rabbit, or anti-sheep IgG antibody; 1 : 500; Vector Laboratories Inc.), followed by avidin-biotin-peroxidase complex (ABC Elite; Vector Laboratories Inc.) for another 1 h. Then the sections were reacted in 0.05 M Tris-HCl buffer (pH 7.6) containing 0.04% diaminobenzidine and 0.002% hydrogen peroxide with (dark brown/purple color) or without (brown color) 0.04% nickel chloride. Images were captured using a light microscope (ACT-1, Nikon Corp., Tokyo, Japan).

Densitometric analysis of αSyn

The density of human αSyn-positive cells was quantified using the NIH Image software (National Institute of Mental Health, Bethesda, MD, USA). Every fourth 20-μm-thick serial section of the brain was immunostained for human αSyn and 10 single cells in the substantia nigra pars compacta (SNpc) randomly selected per section (4–7 sections per mice) were used for densitometric analysis (four mice per group). The two-tailed Student's *t*-test was applied to evaluate the statistical significance of the difference between groups. A p value less than 0.05 denoted the presence of statistically significant difference.

DA cell counting, measurement of striatal dopamine, 2-(3,4-dihydroxyphenyl)acetic acid (DOPAC), and homovanillic acid (HVA)

At first, every eighth 20-μm-thick serial sections of the brain were immunostained for hrGFP (for mice injected with rAAV1-hrGFP) or human αSyn (for mice injected with rAAV1-αSyn). Mice that exhibited foreign protein expression in DA cells in more than half area of the entire rostrocaudal region of the SNpc were used for the following investigations. The rostrocaudal area of the SNpc immunopositive for foreign protein was determined in each mouse and used for DA cell counting (see Table 1). In every fourth serial section, the numbers of TH- and Nissl-positive cells in the SNpc were counted both in the rAAV1-injected and intact sides, as reported previously (Mandir *et al.* 1999; Furuya *et al.* 2004). In brief, SNpc cells with nuclei optimally visible by TH immunostaining, and with nuclei, cytoplasm, and nucleoli prominently stained by Nissl staining were counted. The cell number was counted by an experimenter blinded to the genotypes of mice and rAAV1 groups. The data were expressed as percentage of the contralateral side; i.e., the cell number in the rAAV1-injected side over that in the intact side.

Frozen striatal tissues were sonicated in chilled 0.1 M perchloric acid. The samples were centrifuged (20 000 *g* for 10 min at 4°C) and the resulting supernatants were used for the measurement of dopamine, DOPAC, and HVA concentrations. The HPLC system equipped with a reverse-phase C18 column (150 × 4.6 mm; ODS-100s, Tosoh, Tokyo, Japan) and an eight-electrode coulometric electrochemical detection system (ESA-400, ESA. Inc., Chelmsford, MA, USA) was used. The concentrations of dopamine, DOPAC, and HVA were determined in nanomoles per gram of tissue weight. The data were expressed as percentage of contralateral side; that is, the

Table 1 Number of mice used in the present experiments and transduction efficiencies of rAAV1 vector

	3-month-old, 4-week post-injection		12-month-old, 4-week post-injection	
Mice, rAAV1	Number of mice[a]	Efficiency[b] (%)	Number of mice	Efficiency (%)
Wt-Tg, GFP	6/6	75.1 ± 3.4	5/5	74.7 ± 2.5
Wt-Tg, αSyn	6/7	74.3 ± 7.1	6/6	74.4 ± 4.2
I93M-Tg, GFP	4/6	68.2 ± 2.1	7/7	80.8 ± 1.5
I93M-Tg, αSyn	5/6	75.2 ± 7.9	6/7	70.4 ± 5.1
Non-Tg, αSyn	4/6	76.6 ± 5.9	5/6	68.8 ± 4.6

	3-month-old, 4-week post-injection		3-month-old, 8-week post-injection		3-month-old, 13-week post-injection	
Mice, rAAV1	Number of mice	Efficiency (%)	Number of mice	Efficiency (%)	Number of mice	Efficiency (%)
wild-type, GFP	4/4	77.6 ± 0.9	5/5	79.4 ± 5.9	5/5	76.1 ± 3.7
wild-type, αSyn	4/4	74.8 ± 1.0	5/5	73.2 ± 4.8	6/6	77.2 ± 4.6
gad, GFP	5/5	75.7 ± 0.9	5/5	77.7 ± 9.8	6/6	67.5 ± 2.1
gad, αSyn	5/5	76.1 ± 1.1	5/5	80.4 ± 6.4	7/7	77.2 ± 2.1

[a]Data are number of mice selected for DA cell count over that of total mice injected with rAAV1 vector.
[b]Transduction efficiency of rAAV1 vector was expressed as percentage of total DA cells in the SNpc; *i.e.*, the number of DA cells in the contralateral uninjected side in the area immunopositive for foreign protein relative to that in the entire rostrocaudal extent of the SNpc (mean ± SEM).
Wt-Tg, UCH-L1$^{wild\text{-}type}$-Tg; I93M-Tg, UCH-L1^{Ile93Met}-Tg.

concentration in the rAAV1-injected side over that in the intact side. One-way analysis of variance (ANOVA) followed by Tukey-Kramer's *post hoc* test was applied to evaluate the statistical differences among the groups. A p value less than 0.05 denoted the presence of statistically significant difference.

Results

Co-localization of αSyn and UCH-L1 proteins in nigral Lewy bodies in human PD brain

At first, we performed immunohistochemical analysis for αSyn and UCH-L1 proteins using a midbrain section of a patient with sporadic PD. We found several αSyn- and UCH-L1-double-positive Lewy bodies in the pigmented DA cells in the SN (Fig. 1). αSyn and UCH-L1 proteins co-localized on the halo of Lewy bodies. No fluorescent labeling was detected in the control staining lacking the primary antibodies (data not shown). These results suggested a potential physical and/or functional interaction between the two proteins in human PD brain and prompted us to examine this issue in the experimental animal model of PD.

rAAV1 vector-mediated expression of hrGFP or human αSyn protein in mouse DA neurons

The high-titer viral stocks of rAAV1-hrGFP (6×10^{11} genomes/mL) and rAAV1-αSyn (6×10^{11} genomes/mL) were prepared and injected unilaterally into the SN of 3-month-old UCH-L1$^{wild\text{-}type}$-Tg, UCH-L1^{Ile93Met}-Tg mice, and their non-Tg littermates. At 4-weeks post-injection period, mice were killed and examined for the expression of foreign proteins in the SN by immunohistochemical analysis (Fig. 2). We used a polyclonal antibody that detects hrGFP (green; Fig. 2a–d), a monoclonal antibody (clone LB509) that specifically detects αSyn protein of human origin (green; Fig. 2e–j), and anti-TH antibody that stains DA neurons (red; Fig. 2b, d, f, h, and j). The hrGFP protein was distributed uniformly in DA cell bodies (Fig. 2a and c, arrows) and neuronal processes (Fig. 2a and c, arrowheads) in the SNpc of UCH-L1$^{wild\text{-}type}$-Tg (Fig. 2a and b) and UCH-L1^{Ile93Met}-Tg mice (Fig. 2c and d). On the other hand, virally-introduced human αSyn protein was localized in the cytoplasm, processes (Fig. 2e, g, and i, arrowheads), and perinuclear region (Fig. 2e, g, and i, asterisks) of DA neurons in the SNpc of UCH-L1$^{wild\text{-}type}$-Tg (Fig. 2e and f), UCH-L1^{Ile93Met}-Tg mice (Fig. 2g and h), and non-Tg littermates (Fig. 2i and j). Immunoreactivity for human αSyn was also detected in the intranuclear space in all mice groups (co-localized with DAPI, data not shown), and no major differences were found in the distribution of αSyn protein among the groups. A similar distribution of virally-introduced αSyn was observed in the SNpc DA neurons of 12-month-old Tg and non-Tg mice (data not shown).

Importantly, densitometric analysis of human αSyn in single SNpc cells in these mice showed a significantly higher

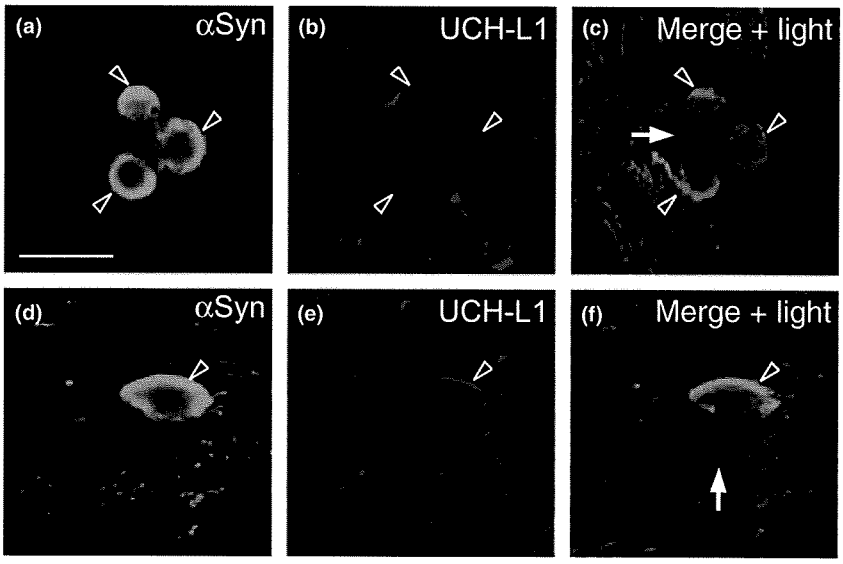

Fig. 1 Immunohistochemical analysis of αSyn and UCH-L1 proteins in the SN of human PD patient. A representative midbrain section of a patient with sporadic PD was immunostained for αSyn (green; a and d) and UCH-L1 proteins (red; b and e). Images were captured using a confocal laser-scanning microscope. Note that several Lewy bodies formed in the pigmented DA neurons (c and f; indicated by white arrows) were double-positive for αSyn and UCH-L1 proteins (a–f; open arrowheads). Scale bar in (a), 20-μm (applicable to a–f).

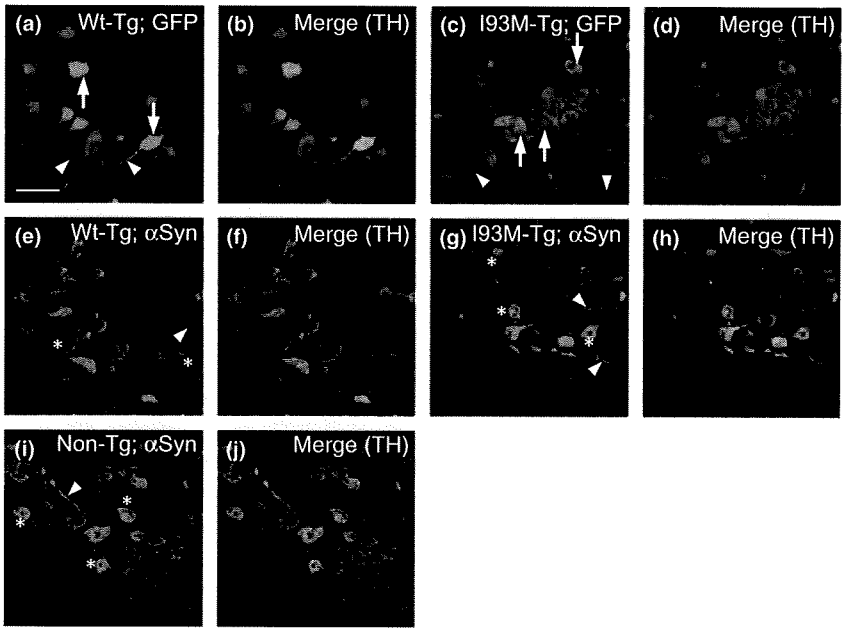

Fig. 2 Recombinant adeno-associated virus (rAAV)-mediated expression of hrGFP and human αSyn protein in mouse DA neurons in the SNpc. The distribution patterns of hrGFP (green; a–d) and αSyn protein (green; e–j) were analyzed in UCH-L1$^{wild\text{-}type}$-Tg (a, b, e, and f; denoted as Wt-Tg), UCH-L1^{Ile93Met}-Tg (c, d, g, and h; I93M-Tg), and non-Tg (i and j; Non-Tg) mice. The DA cell bodies are detected by anti-TH immunostaining (red; b, d, f, h, and j). While hrGFP protein shows a uniform distribution in DA cells and processes (a–d), αSyn is found in cytoplasm, processes (e–j, arrow heads), and perinuclear region (e–j, asterisks) of DA neurons. There are no major differences in the distribution of αSyn among all types of mice examined. Scale bar in (a), 50-μm (applicable to a–j).

immunoreactivity for αSyn in UCH-L1^{Ile93Met}-Tg mice than in UCH-L1$^{wild\text{-}type}$-Tg and non-Tg mice (Fig. 3a–d).

Next, we injected rAAV1-hrGFP or rAAV1-αSyn into the SN of 3-month-old *gad* mice and their wild-type littermates. Similarly, hrGFP protein was distributed uniformly in DA cell bodies and neuronal processes, and αSyn protein was identified in the cytoplasm, processes, perinuclear region, and intranuclear spaces of DA neurons in the SNpc of these mice with no significant difference between the groups (data not shown). As shown in Fig. 4(a)–(c), there was no significant difference in the virally-expressed αSyn between the groups at 13-weeks post-injection, as confirmed by densitometric analysis.

Effect of αSyn over-expression in UCH-L1-Tg mice

Next, we studied the effect of αSyn over-expression on the survival of DA neurons in Tg and non-Tg mice. Every fourth 20-μm-thick serial nigral section was immunostained using anti-TH antibody, followed by Nissl staining. As shown in Fig. 5, loss of DA cell bodies was observed in the SNpc of UCH-L1^{Ile93Met}-Tg mice injected with rAAV1-αSyn (compare Fig. 5e and f, and g and h; indicated by open arrowheads in e) at 4-weeks post-injection. On the other hand, injection of rAAV1-αSyn caused no apparent cell loss in UCH-L1$^{wild\text{-}type}$-Tg (Fig. 5a–d) and non-Tg mice (Fig. 5i–l) at the same time point. Immunostaining for another DA cell marker, dopamine transporter, also showed loss of DA

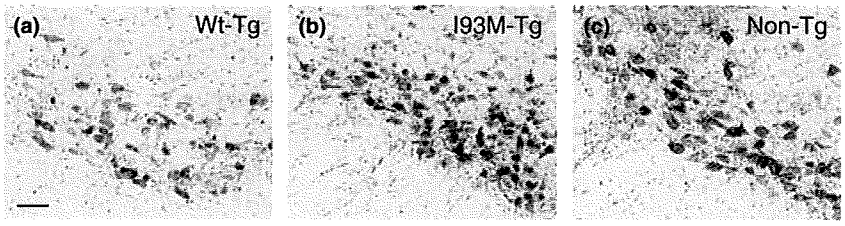

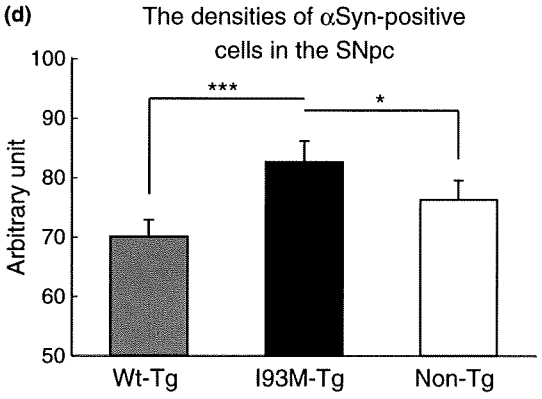

Fig. 3 Densitometric quantification of αSyn in single cells of the SNpc of UCH-L1-Tg and non-Tg mice. Nigral sections were subjected to anti-human αSyn immunostaining. Representative photographs were taken in UCH-L1$^{wild\text{-}type}$-Tg (a; denoted as Wt-Tg), UCH-L1^{Ile93Met}-Tg (b; I93M-Tg), and non-Tg mice (c; Non-Tg). Scale bar in (a), 50-μm (applicable to a–c). (d) The density of human αSyn was quantified using 4–7 of every four serial nigral sections (n = 4 mice for each group). *$p < 0.05$ and ***$p < 0.001$ (two-tailed Student's t-test).

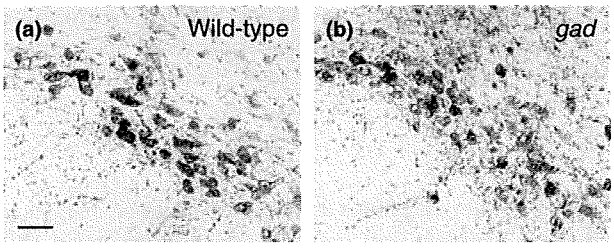

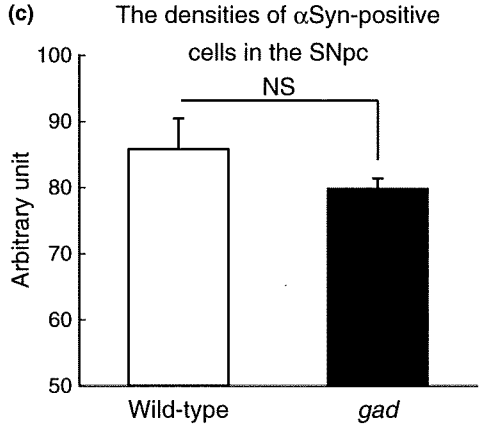

Fig. 4 Densitometric quantification of αSyn in single cells of the SNpc of wild-type and *gad* mice. Nigral sections were subjected to anti-human αSyn immunostaining. Representative photographs were taken in wild-type (a) and *gad* mice (b). Scale bar in (a), 50-μm (applicable to a and b). (c) The density of human αSyn was quantified using 4–7 of every four serial nigral sections (n = 4 mice for each group). n.s., not significant (two-tailed Student's t-test).

cell bodies in the SNpc of UCH-L1^{Ile93Met}-Tg mice injected with rAAV1-αSyn (Fig. 6a–f). Immunostaining of nigral sections of the three genetic types of mice using anti-active caspase-3 antibody showed anti-active caspase-3-immunoreactivities in the SNpc of the rAAV1-αSyn-injected side of UCH-L1^{Ile93Met}-Tg mice (Fig. 6g). These results suggest that αSyn-induced DA cell degeneration in UCH-L1^{Ile93Met}-Tg mice is mediated through apoptotic machinery. Then, we counted the number of TH- and Nissl-positive SNpc cells in both rAAV1-injected and non-injected intact sides of these mice. Immunostaining in the rostrocaudal areas of the SN for hrGFP and human αSyn varied among mice, and accordingly, we determined the immunostaining in each mouse using every eighth 20-μm-thick serial nigral section. Mice positive for the virally-introduced protein in more than half of the rostrocaudal region of the SN were selected for DA cell counting (see Materials and Methods). Table 1 provides a summary of the numbers of selected mice, rAAV1-injected mice, and transduction efficiencies of rAAV1 vector in the selected mice. In Fig. 7(a) and (b), the data are represented as % of contralateral, *i.e.*, TH- and Nissl-positive cell number in the rAAV1-injected side relative to that in the intact side. In rAAV1-αSyn-injected mice (Fig. 7a and b, solid bars), UCH-L1^{Ile93Met}-Tg mice (n = 5, number of animals shown in parenthesis in each bar) exhibited significant loss of DA cell bodies (~30% decrease) compared with UCH-L1$^{wild\text{-}type}$-Tg (~0% decrease) and non-Tg mice (~10% decrease). Furthermore, the relative number of DA cells in the rAAV1-αSyn-injected UCH-L1^{Ile93Met}-Tg mice was significantly lower than in rAAV1-hrGFP-injected UCH-L1^{Ile93Met}-Tg mice (Fig. 7a and b, open bars; ~0% decrease), indicating that the loss of DA cell bodies was mediated specifically by αSyn protein but not by the rAAV1 vector itself or surgical injury. In 12-month-old UCH-L1^{Ile93Met}-Tg mice, we observed a similar extent (~30% decrease) of significant degeneration of TH- and Nissl-positive DA cell bodies,

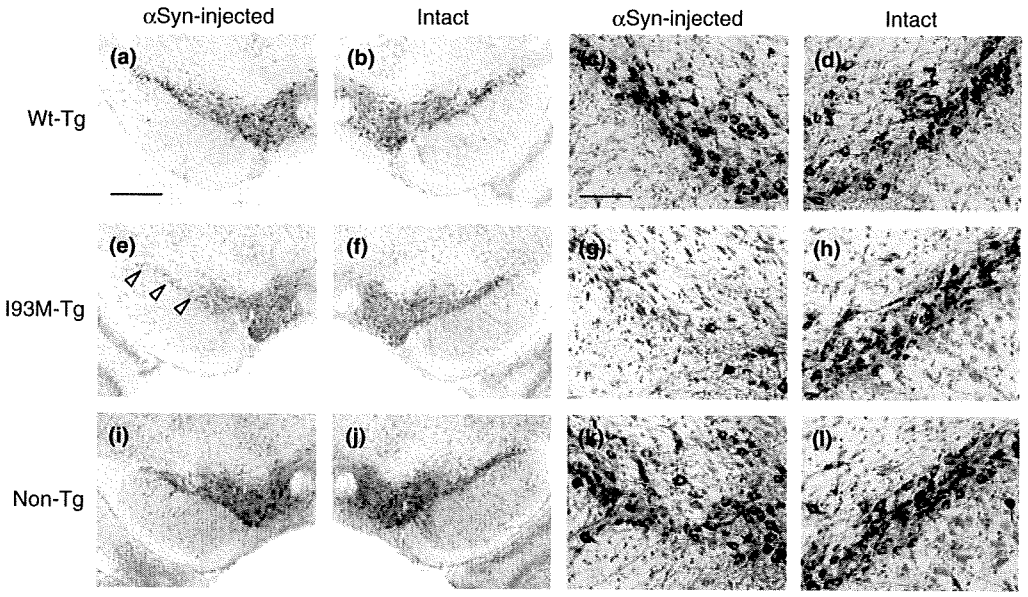

Fig. 5 α-Synuclein-induced degeneration of DA cell bodies in the SNpc of UCH-L1^{Ile93Met}-Tg mice at 4-weeks post-injection. Nigral sections were subjected to anti-TH immunostaining, followed by Nissl staining. Photographs were taken in UCH-L1$^{wild\text{-}type}$-Tg (a–d; denoted as Wt-Tg), UCH-L1^{Ile93Met}-Tg (e–h; I93M-Tg), and non-Tg mice (i–l; Non-Tg) injected with rAAV1-αSyn. The rAAV1-αSyn-injected side (a, c, e, g, i, and k; αSyn-injected) and non-injected intact side (b, d, f, h, j, and l; Intact) are shown. Panels (c), (d), (g), (h), (k), and (l) are enlarged images of (a), (b), (e), (f), (i), and (j), respectively. Note that the DA cell bodies are degenerated in UCH-L1^{Ile93Met}-Tg mice (compare e and f, and g and h; indicated by open arrowheads in e). Scale bar in (a), 500-μm (applicable to a, b, e, f, i, and j); and in (c), 100-μm (to c, d, g, h, k, and l).

which was also specifically induced by αSyn over-expression (Fig. 7a and b).

Next, we measured striatal dopamine concentrations in these mice. However, we could not detect any significant decrease in dopamine concentrations, both in 3- and 12-month-old mice, between the rAAV1-hrGFP- (Fig. 7c, open bars; % of contralateral) and rAAV1-αSyn-injected groups (solid bars) in both UCH-L1$^{wild\text{-}type}$-Tg and UCH-L1^{Ile93Met}-Tg mice, and among the three genetic types of mice in the rAAV1-αSyn-injected groups. There were also no significant changes in the concentrations of dopamine metabolites; DOPAC and HVA (data not shown).

Effects of αSyn over-expression in *gad* mice

Finally, we investigated the effect of viral introduction of αSyn in *gad* and their wild-type littermates. The rAAV1-injected mice were selected for the following investigations based on the criteria described above (see also Table 1). At 13-weeks post-injection period, anti-TH- and Nissl-double-staining of nigral sections manifested an rAAV1-αSyn-induced decrease of DA cell bodies in the SNpc of *gad* (Fig. 8e–h) and wild-type mice (Fig. 8a–d). When the number of the SNpc DA cell bodies was counted, we found that the rAAV1-αSyn-induced DA cell loss was significant both in *gad* and wild-type mice at 13-weeks post-injection period (Fig. 9a and b). We also found that there were no significant differences between the rAAV1-αSyn-injected *gad* and wild-type groups at 4- (~10% decrease, Fig. 9a and b), 8- (~20% decrease), and 13-weeks post-injection (~25% decrease), while the rAAV1-αSyn-induced DA cell loss was not yet significant in *gad* mice compared with the rAAV1-hrGFP-injected group at 8-weeks post-injection.

There was no significant decrease in striatal dopamine concentrations at both 8- and 13-weeks post-injection, between the rAAV1-hrGFP- (Fig. 9c, open bars; % of contralateral) and rAAV1-αSyn-injected groups (solid bars), in both wild-type and *gad* mice, and between wild-type and *gad* mice in the rAAV1-αSyn-injected groups. Furthermore, the level of dopamine metabolites, DOPAC and HVA, were not changed in all groups (data not shown).

Discussion

In the present study, based on the previous findings that αSyn and UCH-L1 proteins interact physically in a cell model of PD (Zhou *et al.* 2004) and normal mammalian brain (Liu *et al.* 2002), and are deposited in Lewy bodies in sporadic cases of PD (Lowe *et al.* 1990; Spillantini *et al.* 1997; Baba *et al.* 1998), we performed a fluorescent double-immunolabeling analysis for the two proteins using a midbrain section of a patient with sporadic PD. Co-localization of αSyn and UCH-L1 proteins in the halo of several Lewy bodies (Fig. 1) encouraged us to examine the potential functional interaction between the two proteins in a mouse model of PD; in

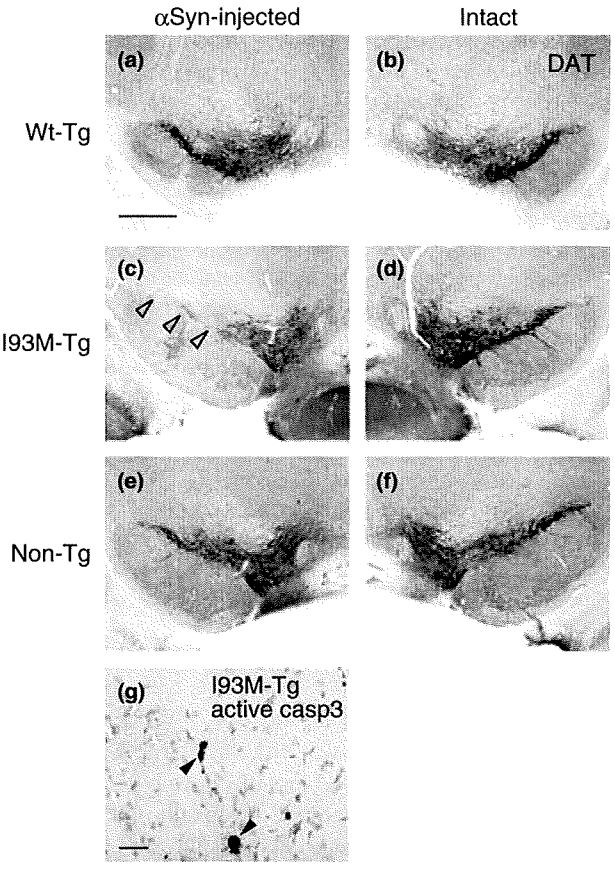

Fig. 6 α-Synuclein-induced degeneration of DA cell bodies examined by anti-DAT- and anti-active caspase-3-immunostaining. Photographs of anti-DAT immunostaining were taken in UCH-L1$^{wild\text{-}type}$-Tg (a, b; denoted as Wt-Tg), UCH-L1^{Ile93Met}-Tg (c, d; I93M-Tg), and non-Tg mice (e, f; Non-Tg) injected with rAAV1-αSyn. The rAAV1-αSyn-injected side (a, c, and e; αSyn-injected) and non-injected intact side (b, d, and f; Intact) are shown. Note the degenerated DA cell bodies in UCH-L1^{Ile93Met}-Tg mice (compare c and d; open arrowheads in c). Immunoreactivity for active caspase-3 (active casp3) is present in the SNpc of UCH-L1^{Ile93Met}-Tg mice injected with rAAV1-αSyn (g; solid arrowheads). Sections were subjected to Nissl counter-staining. Scale bar in (a), 500-μm (applicable to a–f); and in (g) 25-μm.

particular, whether UCH-L1 affects DA neurotoxicity of abnormally accumulated αSyn protein. The αSyn immunoreactivity on the halo of Lewy bodies was consistent with a previous report, which showed localization of αSyn at peripheral portions of Lewy bodies by immunoelectron microscopic analysis (Baba *et al.* 1998). We investigated αSyn-induced DA neurodegeneration in UCH-L1-Tg and -null mice by using the rAAV-mediated gene delivery. In the 4-week-period of rAAV1-mediated αSyn over-expression (shown in Figs 2 and 3), immunoreactivities for human αSyn in single SNpc cells increased significantly in UCH-L1^{Ile93Met}-Tg mice compared with UCH-L1$^{wild\text{-}type}$-Tg and non-Tg mice (Fig. 3). In this regard, we recently reported that the UCH-L1^{Ile93Met} protein inhibits chaperone-mediated autophagy through abnormally enhanced interaction between the UCH-L1 mutant and LAMP-2A protein (Kabuta and Wada 2008; Kabuta *et al.* 2008a). Such abnormal function of UCH-L1^{Ile93Met} protein might have influenced the accumulation of αSyn in the present model. Furthermore, the loss of DA cell bodies was significantly enhanced in the SNpc of UCH-L1^{Ile93Met}-Tg mice, while it was not yet apparent in UCH-L1$^{wild\text{-}type}$-Tg and non-Tg mice at 4-weeks post-injection (Figs 5–7). We also found that αSyn-induced DA neurodegeneration in UCH-L1^{Ile93Met}-Tg mice occurred through an apoptotic mechanism (Fig. 6). In a pilot experiment, we found a significant decrease in the number of nigral DA cell bodies at 8- and 13-weeks post-injection of rAAV1-αSyn, but the number was not significantly different from that of UCH-L1$^{wild\text{-}type}$-Tg, UCH-L1^{Ile93Met}-Tg, and non-Tg mice. Thus, the present results indicate that the DA neurotoxicity of αSyn protein is markedly enhanced in the presence of UCH-L1^{Ile93Met} protein. Furthermore, we found that αSyn over-expression at 13 weeks (Fig. 4) was associated with a significant DA neurodegeneration in *gad* mice, although the extent of DA cell loss was not significantly different than their wild-type littermates (Figs 8 and 9). These results indicate that the αSyn protein-induced DA neurotoxicity is not altered in the absence of UCH-L1$^{wild\text{-}type}$ protein. The striatal levels of dopamine and its metabolites, DOPAC and HVA, did not change during the period of our study (Figs 7c and 9c). In a recent study, Gorbatyuk *et al.* (2008) reported that serotype-5 rAAV-mediated over-expression of human wild-type αSyn caused a significant decrease in the number of TH- and Nissl-positive cells in the SNpc of rats at 8-weeks post-injection, while the striatal level of dopamine showed no significant decrease. Such discrepancy in the rodent models may because of the difficulty of rAAV particles to fully infiltrate the entire rostrocaudal part of the SN (Table 1), as we have suggested in a previous study (Yamada *et al.* 2004). Alternatively, the relatively slow progression of DA neurodegeneration in this model, compared with other drug-induced PD animal models, might have enabled a feedback overproduction of dopamine in the surviving and/or uninfected DA neurons.

Initially, it was reported that the *PARK5*-associated UCH-L1^{Ile93Met} mutant results in ~50% decrease in its ubiquitin hydrolase activity (Leroy *et al.* 1998; Nishikawa *et al.* 2003). Considered with the fact that *PARK5* has so far been identified in only one German kindred, without absolute penetration (Leroy *et al.* 1998), it is debatable whether *PARK5* is caused by a dominant gain-of-toxic-function or haploinsufficiency, *i.e.*, loss-of-function. In this regard, our recent study showed an age-dependent nigrostriatal DA neurodegeneration in a Tg mice line over-expressing human UCH-L1^{Ile93Met} protein (Setsuie *et al.* 2007). Although the level of transgene expression in the UCH-L1^{Ile93Met}-Tg mice line decreased gradually with aging (Setsuie *et al.* 2007) and the number of nigral DA cell bodies in aged UCH-L1^{Ile93Met}-

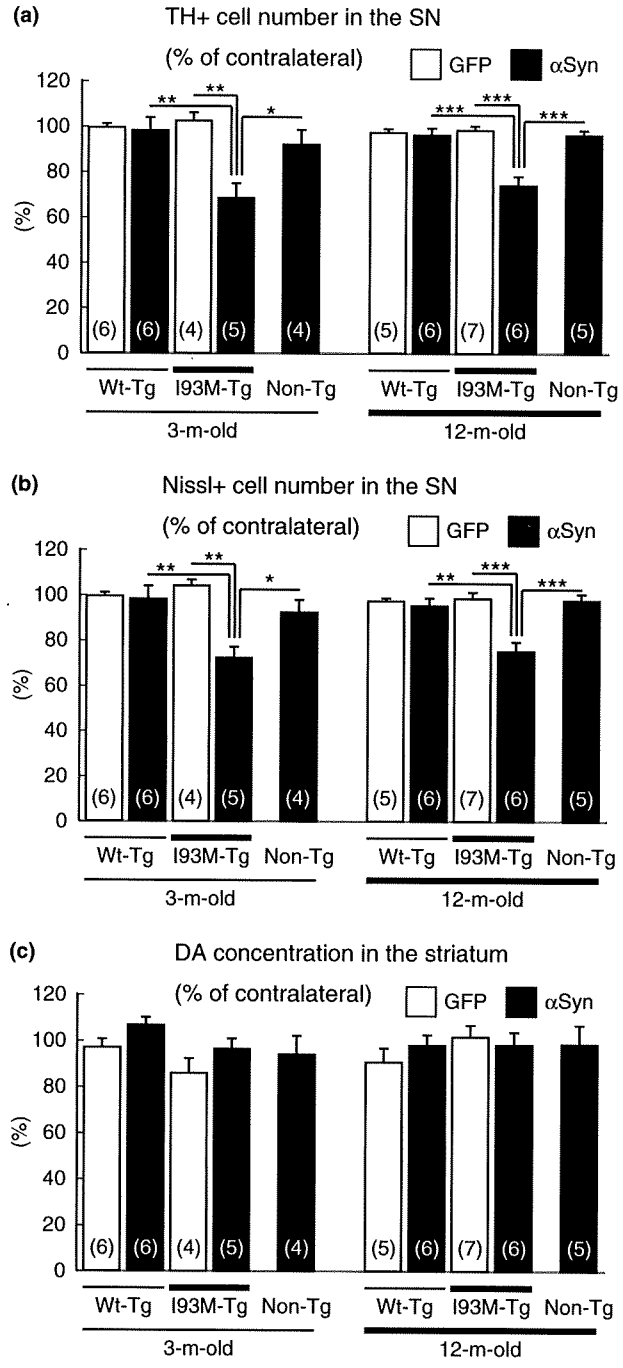

Fig. 7 Dopaminergic cell numbers in the SNpc and dopamine levels in the striatum of UCH-L1-Tg and non-Tg mice at 4-weeks post-injection. The TH- (a) and Nissl-positive cells (b) in the SNpc were counted in 3- and 12-month-old UCH-L1$^{wild\text{-}type}$- (Wt-Tg), UCH-L1^{Ile93Met}-Tg (I93M-Tg), and non-Tg mice (Non-Tg). Data are % of those in the contralateral side. *Open bars:* rAAV1-hrGFP-injected groups, *solid bars:* rAAV1-αSyn-injected groups. The number of analyzed mice in each group is indicated within the bars. Data are mean ± SEM. $^{*}p < 0.05$, $^{**}p < 0.01$, and $^{***}p < 0.001$ (one-way ANOVA followed by Tukey-Kramer's *post hoc* test). Note that the numbers of DA cells are significantly lower in rAAV1-αSyn-injected UCH-L1^{Ile93Met}-Tg mice than in UCH-L1$^{wild\text{-}type}$-Tg and non-Tg mice both in 3- and 12-month-old mice. Significant differences were also found between the rAAV1-hrGFP- and rAAV1-αSyn-injected groups in UCH-L1^{Ile93Met}-Tg mice both at 3- and 12-months of age. (c) The striatal levels of dopamine measured in rAAV1-injected mice. Data are % of those in the contralateral side. *Open bars:* rAAV1-hrGFP-injected groups, *solid bars:* rAAV1-αSyn-injected groups. The number of analyzed mice in each group is indicated within the bars. Data are mean ± SEM. There were no significant differences in dopamine levels among the examined groups.

Tg mice was not significantly different from age-matched non-Tg littermates (data not shown), our present investigation demonstrated that the rAAV1-αSyn-induced DA cell loss was not influenced by the age of UCH-L1^{Ile93Met}-Tg mice. These results also suggest that the DA neurotoxicity of UCH-L1^{Ile93Met} protein alone might be relatively weak in the absence of abnormal accumulation of αSyn. In this regard, a recent study showed no significant change in endogenous αSyn in UCH-L1^{Ile93Met}-Tg mice (Setsuie *et al.* 2007). Based on the finding that the normal aging process is associated with a significant accumulation of αSyn protein in the SN of human brain (Li *et al.* 2004; Chu and Kordower 2007), we speculate that the toxicity of accumulated αSyn might be enhanced by the UCH-L1^{Ile93Met} protein in *PARK5* carriers, leading to a critical loss of DA cells and subsequent development of PD symptoms. The precise mechanism for mutated UCH-L1-mediated toxicity in the presence of accumulated αSyn should be clarified in future studies.

Several studies have reported that the over-expressed αSyn functions as a protective molecule in neuronal cells other than DA neurons (da Costa *et al.* 2000; Xu *et al.* 2002; Chandra *et al.* 2005). The selective vulnerability of DA cells in PD could be explained by the findings that αSyn protein could be covalently bound to dopamine (Conway *et al.* 2001) or could be conformationally changed by interaction with dopaminochrome *in vitro* (Norris *et al.* 2005). Both these mechanisms could lead to altered aggregation propensity, exerting a selective toxicity against culture DA cells (Xu *et al.* 2002), and elevation of intracellular catecholamine level (Mosharov *et al.* 2006). UCH-L1 is also reported to undergo oxidative modification in the brains of patients with PD and Alzheimer's disease (Choi *et al.* 2004). Furthermore, we reported recently that carbonyl-modified UCH-L1 shares aberrant molecular properties with UCH-L1^{Ile93Met}, including similar secondary structural changes, increased insolubility, and elevated interaction with various proteins such as tubulin (Kabuta *et al.* 2008b). We speculate that such post-translational modification, or perhaps another yet unidentified modification(s), could potentially induce the neurotoxic activity of UCH-L1, rendering the accumulated αSyn protein neurotoxic to nigral DA neurons in patients with the sporadic form of PD.

On the other hand, our present study showed that nigral DA cells were killed to no more/lesser extent by the

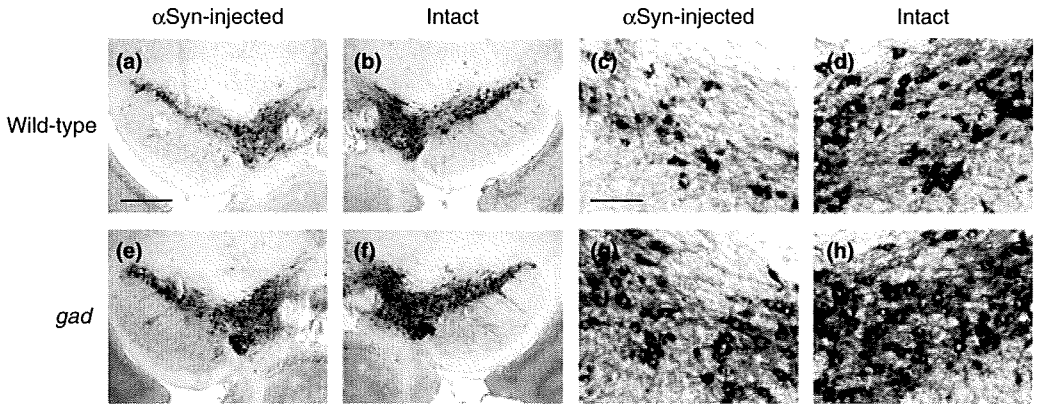

Fig. 8 α-Synuclein-induced degeneration of DA cell bodies in the SNpc of wild-type and *gad* mice at 13-weeks post-injection. Nigral sections were subjected to anti-TH immunostaining, followed by Nissl staining. Photographs were taken in wild-type littermate (a–d) and *gad* mice (e–h) injected with rAAV1-αSyn. The rAAV1-αSyn-injected side (a, c, e, and g; αSyn-injected) and non-injected intact side (b, d, f, and h; Intact) are shown. Panels (c), (d), (g), and (h) are enlarged images of (a), (b), (e), and (f), respectively. Note the degeneration of DA cell bodies in the rAAV1-αSyn-injected sides in both the wild-type and *gad* mice. Scale bar in (a), 500-μm (applicable to a, b, e, and f); and in (c), 100-μm (to c, d, g, and h).

injection of rAAV1-αSyn in the absence of UCH-L1 protein, *i.e.*, in *gad* mice. Previous pathological studies in *gad* mice suggested that UCH-L1 has important roles in the survival of certain neuronal populations, such as sensory and motor neurons (Oda *et al.* 1992; Miura *et al.* 1993). Recent reports also showed that UCH-L1 protein is involved in the survival of other types of neuronal cells. In birds and mice, up-regulation of UCH-L1 is associated with increased survival of replaceable neurons, which continue to be produced and replaced in adulthood (Lombardino *et al.* 2005). Moreover, transduction of exogenous UCH-L1 protein protected against β-amyloid-induced synaptic dysfunction of hippocampal neurons *in vitro* and improved the retention of contextual learning in a mouse model of Alzheimer's disease (Gong *et al.* 2006). As mentioned above, UCH-L1 protein is oxidatively modified and down-regulated in the frontal cortex of patients with sporadic PD and Alzheimer's disease (Choi *et al.* 2004). We reported that oxidation of UCH-L1 protein by 4-hydroxynonenal resulted in a loss of ubiquitin hydrolase activity *in vitro* (Nishikawa *et al.* 2003). In another study, we also reported that UCH-L1 bound to and stabilized monomeric ubiquitin molecule *in vivo*; the level of monomeric ubiquitin was significantly decreased in various brain structures of *gad* mice (Osaka *et al.* 2003). Moreover, proteomic analysis of proteins isolated from the cortical area of *gad* brain revealed oxidative modification of several key proteins possibly linked to neurodegeneration (Castegna *et al.* 2004). However, it is still unknown whether such modification of proteins does occur in the nigral DA cells of *gad* mice. Indeed, no pathological changes have been reported in the SN of *gad* mice. When we counted the number of TH- and Nissl-double-positive DA cells in the entire rostrocaudal extent of the SNpc of *gad* mice, there was no significant difference with wild-type mice (data not shown). Thus, we add an alternative scenario; functional loss of UCH-L1 might have neuroprotective effects. The present study showed that there was no significant decrease in DA cells in *gad* mice between rAAV1-hrGFP-injected and rAAV1-αSyn-injected groups at 8-weeks post-injection, while there was a significant one in wild-type mice (Fig. 9a and b). These results could imply the potential deleterious effects of normal UCH-L1, which were suggested previously by Liu *et al.* (2002). Recently, we reported that retinal neurons in *gad* mice were resistant to ischemic injury (Harada *et al.* 2004). Ischemic stress induces UCH-L1-mediated up-regulation of ubiquitin in wild-type mice, but high levels of ubiquitin induced caspase-dependent retinal neuronal apoptosis (Harada *et al.* 2004). We speculate that another closely related ubiquitin hydrolyzing enzyme, UCH-L3, might have complemented the loss of UCH-L1. The UCH-L1- and UCH-L3-double-null mice show more severe neurodegenerative phenotypes than *gad* mice (Kurihara *et al.* 2001); accordingly, the vulnerability of their nigrostriatal DA neurons to αSyn accumulation should be analyzed in detail in the future. However, the present results demonstrated clearly that the loss of UCH-L1 protein does not cause any harmful or protective effect on prolonged abnormal accumulation of αSyn in nigral DA cells.

In conclusion, our study showed that accumulated αSyn protein is neurotoxic to DA neurons and that such neurotoxicity is enhanced by *PARK5*-associated UCH-L1^{Ile93Met} mutant, but not influenced by the loss of UCH-L1$^{wild\text{-}type}$ protein *in vivo*. Accordingly, we believe that the present results support the hypothesis of dominant gain-of-toxic-function mutation of UCH-L1 as the cause of *PARK5*. Considering the possibility that the UCH-L1$^{wild\text{-}type}$ protein might be toxic by certain age-dependent post-translational

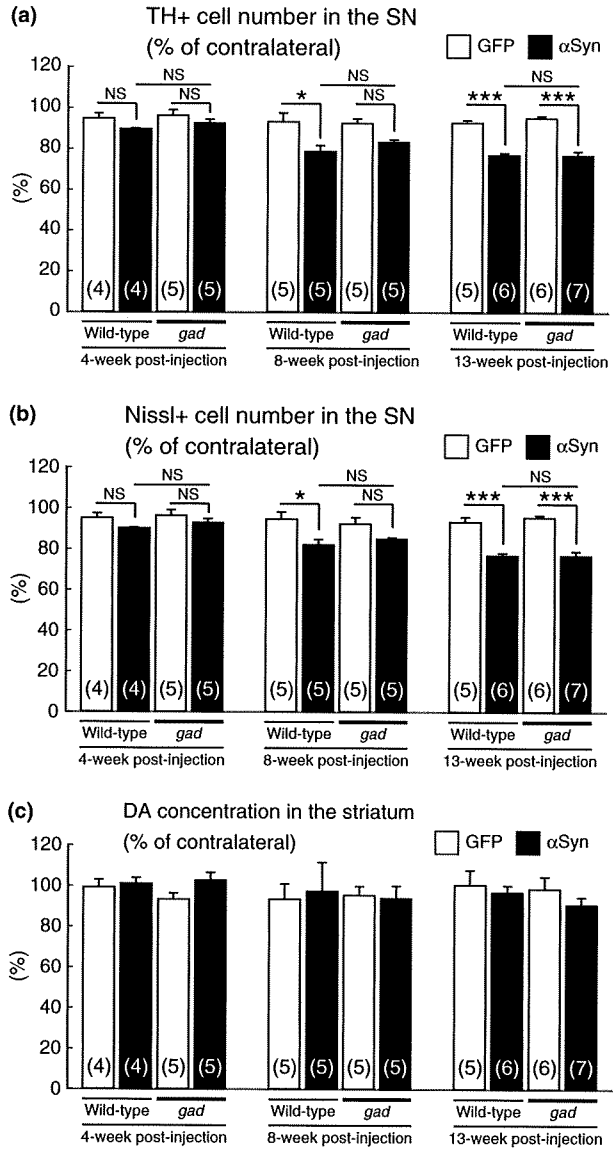

Fig. 9 Dopaminergic cell number in the SNpc and dopamine concentration in the striatum of wild-type and *gad* mice at 4-, 8-, and 13-weeks post-injection. The TH- (a) and Nissl-positive cells (b) in the SNpc were counted in 3-month-old mice. Data are % of the numbers in the contralateral side. *Open bars:* rAAV1-hrGFP-injected groups, *solid bars:* rAAV1-αSyn-injected groups. The number of analyzed mice in each group is indicated within the bars. Data are mean ± SEM. $^{*}p < 0.05$, $^{***}p < 0.001$, and n.s., not significant (one-way ANOVA followed by Tukey-Kramer's *post hoc* test). Note the lack of significant differences between the rAAV1-αSyn-injected wild-type and *gad* groups both at 8- and 13-weeks post-injection. (c) The striatal levels of dopamine were measured in the rAAV1-injected mice. Data are % of the levels in the contralateral side. *Open bars:* rAAV1-hrGFP-injected groups, *solid bars:* rAAV1-αSyn-injected groups. The number of analyzed mice in each group is indicated within the bars. Data are mean ± SEM. There were no significant differences in dopamine levels in the examined groups.

modifications in DA neurons, elucidation of the entire functions of fPD-linked causative gene products and functional interactions among them should provide new insights into the molecular pathogenesis and clinical approaches for the sporadic form of PD.

Acknowledgements

This work was supported by a High Technology Research Center grant, Program for Promotion of Fundamental Studies in Health Sciences of the National Institute of Biomedical Innovation, a Grant-in-Aid for Scientific Research from the Ministry of Education, Culture, Sports, Science and Technology of Japan, and a Grant-in-Aid for Scientific Research from the Ministry of Health, Labour and Welfare of Japan.

References

Baba M., Nakajo S., Tu P. H., Tomita T., Nakaya K., Lee V. M., Trojanowski J. Q. and Iwatsubo T. (1998) Aggregation of alpha-synuclein in Lewy bodies of sporadic Parkinson's disease and dementia with Lewy bodies. *Am. J. Pathol.* **152**, 879–884.

Castegna A., Thongboonkerd V., Klein J., Lynn B. C., Wang Y. L., Osaka H., Wada K. and Butterfield D. A. (2004) Proteomic analysis of brain proteins in the gracile axonal dystrophy (gad) mouse, a syndrome that emanates from dysfunctional ubiquitin carboxyl-terminal hydrolase L-1, reveals oxidation of key proteins. *J. Neurochem.* **88**, 1540–1546.

Chandra S., Gallardo G., Fernandez-Chacon R., Schluter O. M. and Sudhof T. C. (2005) Alpha-synuclein cooperates with CSPalpha in preventing neurodegeneration. *Cell* **123**, 383–396.

Choi J., Levey A. I., Weintraub S. T., Rees H. D., Gearing M., Chin L. S. and Li L. (2004) Oxidative modifications and down-regulation of ubiquitin carboxyl-terminal hydrolase L1 associated with idiopathic Parkinson's and Alzheimer's diseases. *J. Biol. Chem.* **279**, 13256–13264.

Chu Y. and Kordower J. H. (2007) Age-associated increases of alpha-synuclein in monkeys and humans are associated with nigrostriatal dopamine depletion: is this the target for Parkinson's disease? *Neurobiol. Dis.* **25**, 134–149.

Conway K. A., Rochet J. C., Bieganski R. M. and Lansbury P. T. Jr (2001) Kinetic stabilization of the alpha-synuclein protofibril by a dopamine-alpha-synuclein adduct. *Science* **294**, 1346–1349.

da Costa C. A., Ancolio K. and Checler F. (2000) Wild-type but not Parkinson's disease-related ala-53 –> Thr mutant alpha-synuclein protects neuronal cells from apoptotic stimuli. *J. Biol. Chem.* **275**, 24065–24069.

Farrer M. J. (2006) Genetics of Parkinson disease: paradigm shifts and future prospects. *Nat. Rev. Genet.* **7**, 306–318.

Furuya T., Hayakawa H., Yamada M., Yoshimi K., Hisahara S., Miura M., Mizuno Y. and Mochizuki H. (2004) Caspase-11 mediates inflammatory dopaminergic cell death in the 1-methyl-4-phenyl-1,2,3,6-tetrahydropyridine mouse model of Parkinson's disease. *J. Neurosci.* **24**, 1865–1872.

Gong B., Cao Z., Zheng P., Vitolo O. V., Liu S., Staniszewski A., Moolman D., Zhang H., Shelanski M. and Arancio O. (2006) Ubiquitin hydrolase Uch-L1 rescues beta-amyloid-induced decreases in synaptic function and contextual memory. *Cell* **126**, 775–788.

Gorbatyuk O. S., Li S., Sullivan L. F., Chen W., Kondrikova G., Manfredsson F. P., Mandel R. J. and Muzyczka N. (2008) The

phosphorylation state of Ser-129 in human alpha-synuclein determines neurodegeneration in a rat model of Parkinson disease. *Proc. Natl Acad. Sci. USA* **105**, 763–768.

Harada T., Harada C., Wang Y. L. *et al.* (2004) Role of ubiquitin carboxy terminal hydrolase-L1 in neural cell apoptosis induced by ischemic retinal injury in vivo. *Am. J. Pathol.* **164**, 59–64.

Kabuta T. and Wada K. (2008) Insights into links between familial and sporadic Parkinson's disease: physical relationship between UCH-L1 variants and chaperone-mediated autophagy. *Autophagy* **4**, 827–829.

Kabuta T., Furuta A., Aoki S., Furuta K. and Wada K. (2008a) Aberrant interaction between Parkinson's disease-associated mutant UCH-L1 and the lysosomal receptor for chaperone-mediated autophagy. *J. Biol. Chem.* **283**, 23731–23738.

Kabuta T., Setsuie R., Mitsui T., Kinugawa A., Sakurai M., Aoki S., Uchida K. and Wada K. (2008b) Aberrant molecular properties shared by familial Parkinson's disease-associated mutant UCH-L1 and carbonyl-modified UCH-L1. *Hum. Mol. Genet.* **17**, 1482–1496.

Kirik D., Rosenblad C., Burger C., Lundberg C., Johansen T. E., Muzyczka N., Mandel R. J. and Bjorklund A. (2002) Parkinson-like neurodegeneration induced by targeted overexpression of alpha-synuclein in the nigrostriatal system. *J. Neurosci.* **22**, 2780–2791.

Kirik D., Annett L. E., Burger C., Muzyczka N., Mandel R. J. and Bjorklund A. (2003) Nigrostriatal alpha-synucleinopathy induced by viral vector-mediated overexpression of human alpha-synuclein: a new primate model of Parkinson's disease. *Proc. Natl Acad. Sci. USA* **100**, 2884–2889.

Kruger R., Kuhn W., Muller T., Woitalla D., Graeber M., Kosel S., Przuntek H., Epplen J. T., Schols L. and Riess O. (1998) Ala30Pro mutation in the gene encoding alpha-synuclein in Parkinson's disease. *Nat. Genet.* **18**, 106–108.

Kurihara L. J., Kikuchi T., Wada K. and Tilghman S. M. (2001) Loss of Uch-L1 and Uch-L3 leads to neurodegeneration, posterior paralysis and dysphagia. *Hum. Mol. Genet.* **10**, 1963–1970.

Larsen C. N., Price J. S. and Wilkinson K. D. (1996) Substrate binding and catalysis by ubiquitin C-terminal hydrolases: identification of two active site residues. *Biochemistry* **35**, 6735–6744.

Larsen C. N., Krantz B. A. and Wilkinson K. D. (1998) Substrate specificity of deubiquitinating enzymes: ubiquitin C-terminal hydrolases. *Biochemistry* **37**, 3358–3368.

Leroy E., Boyer R., Auburger G. *et al.* (1998) The ubiquitin pathway in Parkinson's disease. *Nature* **395**, 451–452.

Li W., Lesuisse C., Xu Y., Troncoso J. C., Price D. L. and Lee M. K. (2004) Stabilization of alpha-synuclein protein with aging and familial Parkinson's disease-linked A53T mutation. *J. Neurosci.* **24**, 7400–7409.

Liu Y., Fallon L., Lashuel H. A., Liu Z. and Lansbury P. T. Jr (2002) The UCH-L1 gene encodes two opposing enzymatic activities that affect alpha-synuclein degradation and Parkinson's disease susceptibility. *Cell* **111**, 209–218.

Lo Bianco C., Ridet J. L., Schneider B. L., Deglon N. and Aebischer P. (2002) Alpha-synucleinopathy and selective dopaminergic neuron loss in a rat lentiviral-based model of Parkinson's disease. *Proc. Natl Acad. Sci. USA* **99**, 10813–10818.

Lombardino A. J., Li X. C., Hertel M. and Nottebohm F. (2005) Replaceable neurons and neurodegenerative disease share depressed UCHL1 levels. *Proc. Natl Acad. Sci. USA* **102**, 8036–8041.

Lowe J., McDermott H., Landon M., Mayer R. J. and Wilkinson K. D. (1990) Ubiquitin carboxyl-terminal hydrolase (PGP 9.5) is selectively present in ubiquitinated inclusion bodies characteristic of human neurodegenerative diseases. *J. Pathol.* **161**, 153–160.

Mandir A. S., Przedborski S., Jackson-Lewis V., Wang Z. Q., Simbulan-Rosental C. M., Smulson M. E., Hoffman B. E., Guastella D. B., Dawson V. L. and Dawson T. M. (1999) Poly(ADP-ribose) polymerase activation mediates 1-methyl-4-phenyl-1,2,3,6-tetrahydropyridine (MPTP)-induced parkinsonism. *Proc. Natl Acad. Sci. USA* **96**, 5774–5779.

Miura H., Oda K., Endo C., Yamazaki K., Shibasaki H. and Kikuchi T. (1993) Progressive degeneration of motor nerve terminals in GAD mutant mouse with hereditary sensory axonopathy. *Neuropathol. Appl. Neurobiol.* **19**, 41–51.

Mosharov E. V., Staal R. G., Bove J. *et al.* (2006) Alpha-synuclein overexpression increases cytosolic catecholamine concentration. *J. Neurosci.* **26**, 9304–9311.

Nishikawa K., Li H., Kawamura R. *et al.* (2003) Alterations of structure and hydrolase activity of parkinsonism-associated human ubiquitin carboxyl-terminal hydrolase L1 variants. *Biochem. Biophys. Res. Commun.* **304**, 176–183.

Nishioka K., Hayashi S., Farrer M. J. *et al.* (2006) Clinical heterogeneity of alpha-synuclein gene duplication in Parkinson's disease. *Ann. Neurol.* **59**, 298–309.

Norris E. H., Giasson B. I., Hodara R., Xu S., Trojanowski J. Q., Ischiropoulos H. and Lee V. M. (2005) Reversible inhibition of alpha-synuclein fibrillization by dopaminochrome-mediated conformational alterations. *J. Biol. Chem.* **280**, 21212–21219.

Oda K., Yamazaki K., Miura H., Shibasaki H. and Kikuchi T. (1992) Dying back type axonal degeneration of sensory nerve terminals in muscle spindles of the gracile axonal dystrophy (GAD) mutant mouse. *Neuropathol. Appl. Neurobiol.* **18**, 265–281.

Osaka H., Wang Y. L., Takada K. *et al.* (2003) Ubiquitin carboxy-terminal hydrolase L1 binds to and stabilizes monoubiquitin in neuron. *Hum. Mol. Genet.* **12**, 1945–1958.

Polymeropoulos M. H., Lavedan C., Leroy E. *et al.* (1997) Mutation in the alpha-synuclein gene identified in families with Parkinson's disease. *Science* **276**, 2045–2047.

Ramirez A., Heimbach A., Grundemann J. *et al.* (2006) Hereditary parkinsonism with dementia is caused by mutations in ATP13A2, encoding a lysosomal type 5 P-type ATPase. *Nat. Genet.* **38**, 1184–1191.

Saigoh K., Wang Y. L., Suh J. G. *et al.* (1999) Intragenic deletion in the gene encoding ubiquitin carboxy-terminal hydrolase in gad mice. *Nat. Genet.* **23**, 47–51.

Sambrook J. and Russell D. W. (2001) *Molecular Cloning: A Laboratory Manual*, 3rd edn. Cold Spring Harbor Laboratory Press, Cold Spring Harbor, NY.

Setsuie R., Wang Y. L., Mochizuki H. *et al.* (2007) Dopaminergic neuronal loss in transgenic mice expressing the Parkinson's disease-associated UCH-L1 I93M mutant. *Neurochem. Int.* **50**, 119–129.

Singleton A. B., Farrer M., Johnson J. *et al.* (2003) Alpha-synuclein locus triplication causes Parkinson's disease. *Science* **302**, 841.

Spillantini M. G., Schmidt M. L., Lee V. M., Trojanowski J. Q., Jakes R. and Goedert M. (1997) Alpha-synuclein in Lewy bodies. *Nature* **388**, 839–840.

Wilkinson K. D., Lee K. M., Deshpande S., Duerksen-Hughes P., Boss J. M. and Pohl J. (1989) The neuron-specific protein PGP 9.5 is a ubiquitin carboxyl-terminal hydrolase. *Science* **246**, 670–673.

Xu J., Kao S. Y., Lee F. J., Song W., Jin L. W. and Yankner B. A. (2002) Dopamine-dependent neurotoxicity of alpha-synuclein: a mechanism for selective neurodegeneration in Parkinson disease. *Nat. Med.* **8**, 600–606.

Yamada M., Iwatsubo T., Mizuno Y. and Mochizuki H. (2004) Overexpression of alpha-synuclein in rat substantia nigra results in loss of dopaminergic neurons, phosphorylation of alpha-synuclein and activation of caspase-9: resemblance to pathogenetic changes in Parkinson's disease. *J. Neurochem.* **91**, 451–461.

Yasuda T., Miyachi S., Kitagawa R. *et al.* (2007) Neuronal specificity of alpha-synuclein toxicity and effect of Parkin co-expression in primates. *Neuroscience* **144**, 743–753.

Zarranz J. J., Alegre J., Gomez-Esteban J. C. *et al.* (2004) The new mutation, E46K, of alpha-synuclein causes Parkinson and Lewy body dementia. *Ann. Neurol.* **55**, 164–173.

Zhou Y., Gu G., Goodlett D. R., Zhang T., Pan C., Montine T. J., Montine K. S., Aebersold R. H. and Zhang J. (2004) Analysis of alpha-synuclein-associated proteins by quantitative proteomics. *J. Biol. Chem.* **279**, 39155–39164.

Experimental Neurology 221 (2010) 175–185

Contents lists available at ScienceDirect

Experimental Neurology

journal homepage: www.elsevier.com/locate/yexnr

Chronic stress-mutated presenilin 1 gene interaction perturbs neurogenesis and accelerates neurodegeneration

Shohko Kunimoto [a,*], Shun Nakamura [a,1], Keiji Wada [b], Takayoshi Inoue [a]

[a] Department of Biochemistry and Cellular Biology, National Institute of Neuroscience, National Center of Neurology and Psychiatry, Tokyo 187-8502, Japan
[b] Department of Degenerative Neurological Diseases, National Institute of Neuroscience, National Center of Neurology and Psychiatry, Tokyo 187-8502, Japan

ARTICLE INFO

Article history:
Received 30 July 2009
Revised 23 October 2009
Accepted 28 October 2009
Available online 4 November 2009

Keywords:
Neurodegenerative disease
Gene–environment interaction
Chronic intermittent restraint stress (CIRS)
Doublecortin (DCX)
Presenilin 1 (PS1)
Neurogenesis

ABSTRACT

Recent evidence suggests that supplemental factors coincident with aging and genetic determinants might be involved in the initial progression of Alzheimer's disease (AD). Early studies also indicate that chronic stress decreases hippocampal neurogenesis. Here, we investigate the effect of chronic stress on hippocampal neurogenesis using a transgenic mouse line (Tg) that overexpresses human presenilin 1 (PS1) with a familial AD (FAD)-related mutation in order to elucidate how the combination of chronic stress and mutated genes affects the cytoarchitecture in the hippocampal granule cell layer (GCL), which contributes to spatial learning and memory. Using an original chronic intermittent restraint stress (CIRS) protocol, we examined the effect of stress on hippocampal neurogenesis and neurodegeneration by immunohistochemical analysis. After short-term CIRS, neurodegeneration in Tg mice was significantly increased in the hippocampus with an earlier onset and progression than in the non-stressed Tg mice. Moreover, after long-term CIRS, transitional neurodegeneration appeared to proceed along the neuronal circuit involved in cognitive function in stressed Tg mice. Although the number of Pax6-positive (+) cells (mostly granule neuron precursors) did not significantly decrease during CIRS in both non-Tg and Tg mice, doublecortin (DCX) + neuronal progenitor cells in the GCL were markedly influenced in Tg mice; they were significantly reduced without stress compared with non-stressed non-Tg mice and significantly increased by CIRS compared with non-stressed Tg mice. We conclude from these results that diverse responses against stressful experiences among genetically predisposed individuals could lead to cognitive dysfunction through retardation of neuronal maturation and neurodegeneration.

Introduction

In human aging processes, frontal–striatal structural changes of the brain have been suggested to underlie mild memory difficulties. In Alzheimer's disease (AD) patients, cellular pathology characterized by amyloid plaques/neurofibrillary tangles (Golde et al., 2000; Mattson, 2004) results in progressive neurodegeneration and atrophy within medial temporal brain structures that associate with cognitive functions (Jack et al., 1992; Killiany et al., 1993); this leads directly to memory impairment via separate mechanisms (Buckner, 2004). At the molecular level, genetic mutations of presenilin 1 and 2 (PS1, PS2) or missense mutations in amyloid precursor protein increase amyloid β deposition, which are well investigated pathogenic traits of AD (Masters and Beyreuther, 1998). In addition, recent studies have highlighted the significance of adult neurogenesis in the hippocampal granule cell layer (GCL) for cognitive memory (Bruel-Jungerman et al., 2005; Drapeau et al., 2003; Gould et al., 1999; Imayoshi et al., 2008; Kempermann and Gage, 2002; Shors et al., 2001; Zhang et al., 2008), and an acceleration of neurogenesis has indeed been expected to provide therapeutic measures against cognitive impairment in AD (Kuhn et al., 2007; Ogita et al., 2005). In light of the progressive neurodegeneration seen in AD patients, even with increased generation of neuronal progenitor cells in the GCL (Jin et al., 2004), the elucidation of additional factors in granule cell regeneration is essential for clinical applications.

Several lines of evidence have thus far implied a correlation between the stress-induced decrease in hippocampal neurogenesis and deficits in the hippocampus-related memory (Gould and Tanapat, 1999; Nagata et al., 2009; Pardon and Rattray, 2008; Sandi, 2004;

Abbreviations: BrdU, 5-bromo-2′-deoxyuridine; AD, Alzheimer's disease; ANOVA, analysis of variance; CIRS, chronic intermittent restraint stress; CA3, Cornus Ammonis 3; DG, dentate gyrus; DCX, doublecortin; FAD, familial Alzheimer's disease; GCL, granule cell layer; NS, non-stressed control mice; PBS, phosphate buffered saline; PCtx, piriform cortex; +, positive; PS1, presenilin 1; RCtx, retrosplenial cortex; SEM, standard error of the mean; ST, stressed mice; SGZ, subgranular zone; L/V-Tg, transgenic mouse model of AD with overexpression of an FAD-type PS1; non-Tg, transgenic-negative mouse; W, week-old.

* Corresponding author. Present address: Department of Vascular Dementia Research, National Institute for Longevity Sciences, National Center for Geriatrics and Gerontology, 36-3 Gengo, Morioka-machi, Obu City, Aichi 474-8522, Japan. Fax: +81 562 46 8438.
E-mail address: kunimoto@nils.go.jp (S. Kunimoto).
[1] Present Address: Department of Biotechnology and Life Science, Tokyo University of Agriculture and Technology, 2-24-16 Naka-chou, Koganei-city, Tokyo 184-8588, Japan.

0014-4886/$ – see front matter © 2009 Elsevier Inc. All rights reserved.
doi:10.1016/j.expneurol.2009.10.020

Veena et al., 2009). Furthermore, chronic stress accelerates cognitive impairments and increases amyloid deposition in APPV717I-CT100 mice overexpressing the familial AD (FAD) V717I "London" mutation within the carboxyl terminus of human amyloid precursor protein (Jeong et al., 2006). However, the combinatorial effect of chronic stress and mutated genes on the hippocampal neurogenesis is not fully understood. Here we hypothesize that, in individuals predisposed to genetic mutations for AD, a mutated gene–environmental stress interaction might synergistically deteriorate the level of hippocampal neurogenesis, leading to precocious cognitive impairment. To test this hypothesis, we selected a transgenic mouse model of AD with overexpression of an FAD-type PS1 (L286V) (L/V-Tg); these mice accumulate abnormal amyloid β in the cytoplasm to bring about massive cell degeneration without formation of amyloid plaques after 6 months of age (Chui et al., 1999). We exposed this genetically predisposed mouse to stressful environments and found that the number of degenerating neurons was increased in the brain regions involved in cognitive function (i.e., the hippocampus) earlier in stressed mice than in non-stressed mice, and neurogenesis was affected differently by stress in the Tg and non-Tg mice. These data suggest that diverse responses to stressful experiences among genetically predisposed individuals might affect neurogenesis and neurodegeneration. We propose that mice that display hallmarks of AD late in life with conditioned environmental factors could be used as an animal model for the analysis of the onset and progression of AD.

Materials and methods

Animals

A transgenic mouse line overexpressing human PS1 with an FAD-related mutation of leucine 286 to valine (L286V) under the control of the human PDGF-β promoter (Chui et al., 1999) had been originally produced by Dr. Chui et al. at the National Institute of Neuroscience (NCNP, Tokyo, Japan). The mouse line was maintained in the FVB/N background and was back-crossed to obtain male hemizygous mice (L/V-Tg) at the NCNP. In the brains of transgenic mice older than 13 months (aged mice), neurodegeneration was significantly accelerated without amyloid plaque formation, whereas most populations of neurons deposit amyloid β42 intracellularly. Mice were housed under controlled conditions (21 °C room temperature, 60% humidity, lights on from 8:00 am to 8:00 pm) with food and water available *ad libitum*. Sixty-two young adult (7-week-old) male mice were used in the whole study. All studies were performed by comparing the L/V-Tg mice with the age-matched, transgenic-negative littermates (non-Tg). The Non-Tg and L/V-Tg mice were randomly assigned to the control (NS) or stressed (ST) group [for short-term experiments, non-Tg(NS) ($n=12$), non-Tg(ST) ($n=12$), L/V-Tg(NS) ($n=13$), L/V-Tg (ST) ($n=13$); for long-term experiments, non-Tg(NS) ($n=3$), non-Tg(ST) ($n=3$), L/V-Tg(NS) ($n=3$), L/V-Tg(ST) ($n=3$)]. Animal care and handling were in accordance with institutional regulations and were approved by the Animal Investigation Committee of the National Institute of Neuroscience, Japan, which in turn conforms to the National Institutes of Health guidelines for the care and use of laboratory animals. The number of animals in this study was the minimum required to obtain statistically significant results. The animals were appropriately treated and anesthetized with Nembutal (Dainippon Sumitomo Pharma Co., Osaka, Japan, 0.25 mg/g of pentobarbitone) to minimize their suffering.

Chronic intermittent restraint stress (CIRS)

Young adult (7-week-old) male mice weighing 25.4±0.5 g for L/V-Tg mice and 24.4±0.5 g for non-Tg mice at the beginning of the stress procedure were used. Mice were housed two to three per cage and were habituated to the experimental room for 10 days without handling. The stressed animals were exposed to restraint stress from 9:30 am to 3:30 pm in their home cage using a well-ventilated restraint tube that fit closely to the mice (Supplementary Fig. 1). For chronic intermittent restraint stress (CIRS), the experimental mice were put into restraint tubes for 6 h every day for 3 weeks (short-term experiments) or 15 weeks (long-term experiments), excluding the weekends (restrained Monday through Friday, rest from 3:30 pm on Friday to 9:30 am on the next Monday). The animals at 11-week-old (short-term) or 23-week-old (long-term) were sacrificed 1 day after the last session (Saturday; Fig. 1). The control mice (NS) were left in their home cage except for handling during weighing and were sacrificed at the same time as the experimental mice (we considered the NS a handled control). Body weight gain was monitored throughout the experiment (three times a week) and, upon termination, the adrenal glands were removed and weighed.

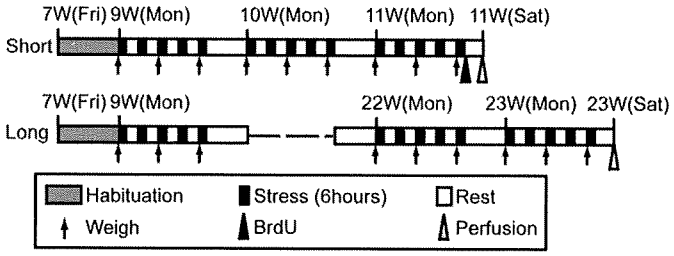

Fig. 1. Protocol summary for short-term (upper) and long-term (lower) chronic intermittent restraint stress (CIRS). For CIRS, each mouse was put into a restraint tube for 6 h every day for 3 weeks (short-term) or 15 weeks (for long-term), excluding weekends, and sacrificed 1 day after the last session (Saturday). For 5-bromo-2′-deoxyuridine (BrdU) labeling, the mice were injected intraperitoneally with BrdU 20 h (for short-term) before perfusion. Fri, Friday; Mon, Monday; Sat, Saturday; W, week-old.

Fixation and histological processing

The animals were perfused transcardially with phosphate buffered saline (PBS, 0.1 M, pH 7.4) followed by 4% paraformaldehyde in PBS. The brains were sagittally cut into halves for post-fixation overnight in the same fixative at 4 °C. The samples were washed in PBS and transferred to an antigen retrieval solution [10 mM sodium citrate, pH 6.0 (Ino, 2003)] for overnight incubation at 4 °C. The samples were then immersed in 300 ml of preheated (95 °C) retrieval solution for 3 min. They were immediately placed in cold 30% sucrose in PBS and incubated at 4 °C overnight. The blocks were immersed in Tissue-Tek OCT Compound (Sakura Fine Technical, Tokyo, Japan), frozen with dry ice, and stored at −80 °C. Cryosections (40 μm thick) cut frontally through the hippocampus using a sliding microtome (Leica CM3000, Leica Microsystems, Bannockburn, IL, USA) were collected sequentially into eight series in a cryoprotectant solution [ethyleneglycol: glycerol:PBS (1:1:2, v/v)] and stored at −20 °C.

Silver staining

For the staining of degenerating neurons, we prepared 8–10 sections from the short-term group [non-Tg(NS) ($n=2$), non-Tg(ST) ($n=2$), L/V-Tg(NS) ($n=2$), L/V-Tg(ST) ($n=2$)] and 12–14 sections from the long-term group [non-Tg(NS) ($n=3$), non-Tg(ST) ($n=3$), L/V-Tg(NS) ($n=3$), L/V-Tg(ST) ($n=3$)]. The mice were perfused as described above. The whole brains were post-fixed for 48 h at 4 °C. Right brain hemispheres were immersed in an embedding medium, frozen with dry ice and stored at −80 °C. Silver staining of cryostat sections was performed using an FD NeuroSilver Kit II (FD NeuroTechnologies, Ellicott City, MD, U.S.A.) according to the manufacturer's protocol to detect degenerating neurons. Sections [Bregma −1.58~−2.92 (Paxinos and Franklin, 2001)] viewed on a video monitor connected to a LEICA DM2500 microscope (×20 NA

0.40 objective) with a LEICA DFC 300-FX digital camera were used for cell counting. The degenerating cells in the dentate gyrus (DG), Cornus Ammonis 3 (CA3), retrosplenial cortex (RCtx), and piriform cortex (PCtx) were counted using the analyze particle mode of Object-Image2.15 (US National Institutes of Health and at the University of Amsterdam). The analytical process was as follows: microscopic color images (each 0.16 mm^2) were opened using the Object-Image2.15 software and through a red channel image, degenerating neurons were selected by density slice mode. The degenerating neurons were always indicated by dense silver precipitates, which appear as black grains in their somata and cells with numerous fine grains in their somata and were counted using the analyze particles mode with several optional settings (i.e. 'minimal particle size of 20 pixels,' 'label particles,' 'outline particles,' 'ignore particles touching edge,' and 'include interior holes'). The numerical density of the degenerating cells was converted to a percentage of the cell number in non-Tg(NS) mice.

Immunohistochemical analysis

Serial sections (40 μm thick) were processed for immunostaining using a primary antibody against Pax6 (Inoue et al., 2000) (anti-Pax6 rabbit antibody 63, 1:500) [non-Tg(NS) ($n=5$), non-Tg(ST) ($n=5$), L/V-Tg(NS) ($n=5$), L/V-Tg(ST) ($n=5$)], Ki-67 (anti-Ki-67 rabbit serum, 1:50;YLEM, Roma, Italy, #PRO229) [non-Tg(NS) ($n=7$), non-Tg(ST) ($n=6$), L/V-Tg(NS) ($n=7$), L/V-Tg(ST) ($n=6$)], or double-cortin (DCX) (anti-DCX guinea pig antibody, 1:3000; Chemicon, CA, USA, #AB5910) [non-Tg(NS) ($n=9$), non-Tg(ST) ($n=8$), L/V-Tg(NS) ($n=9$), L/V-Tg(ST) ($n=8$)]. Free-floating sections were treated first with PBS containing 10% methanol and 3% H_2O_2 for 30 min at room temperature and rinsed in PBS. The sections were next treated with 3% normal goat serum in PBS containing 0.1% Triton X-100 for 2 h at room temperature and incubated for 48 h in the primary antibody solution at 4 °C. Then they were incubated with biotinylated goat anti-rabbit IgG (1:5000; Vector, CA, USA, #BA-1000) for Pax6 and Ki-67 or biotinylated goat anti-guinea pig IgG (1:500; Vector #BA-7000) for DCX for 2 h at room temperature. The immunoreactions with the ABC reagent (Vector) and the ImmunoPure Methal Enhanced DAB Substrate Kit (PIERCE, Rockford, IL, USA) were done according to the manufacturer's protocol. The sections were placed onto an MAS-coated slide glass (Matsunami, Osaka, Japan, #S9443), air-dried, dehydrated with ethanol and xylene, and coverslipped with HSR solution (International Reagents Corp., Kobe, Japan).

BrdU labeling

For the labeling of mitotic cells, the mice received an intraperitoneal injection of 5-bromo-2′-deoxyuridine (BrdU, Sigma, 15 mg/ml dissolved in 0.9% NaCl, 20 μl/g body weight) at 4:30–5:00 pm and were perfused 20 h after injection [non-Tg(NS) ($n=5$), non-Tg(ST) ($n=4$), L/V-Tg(NS) ($n=5$), L/V-Tg(ST) ($n=5$)]. This high dose of BrdU (300 mg/kg) is a specific, quantitative, and nontoxic marker of dividing cells in the adult DG (Cameron and McKay, 2001). Free-floating sections (40 μm thick) were made and incubated in 2 N HCl for 30 min at 37 °C. After being rinsed in borate buffer and PBS, sections were incubated with an anti-BrdU rat monoclonal antibody (1:500, abcam, Cambridge, MA, USA, #ab6326) overnight at 4 °C and then with the secondary antibody for 2 h at room temperature. The immunoreactions with the ABC reagent and DAB were performed as described above.

Quantification and stereology

Serial sections [six sections from each animal, Bregma −1.34 to −3.08 (Paxinos and Franklin, 2001)] (Supplementary Fig. 2) of one hemisphere were taken for stereological quantification of the dentate GCL, including the Pax6-, Ki-67-, DCX-, and BrdU-positive cells in the GCL and subgranular zone (SGZ, a two-cell-thick layer in the granule cell layer, is located close to the hilus or in the lower part of the GCL). For Pax6 or Ki-67 immunostaining, toluidine blue-stained serial sections were used to determine the total volume of the GCL. DAB-stained individual sections were viewed on a video monitor connected to a Zeiss Axiophot 2 microscope (2.5× NA 0.12 objective) with a 3CCD Fuji (Fujifilm, Tokyo, Japan) digital camera. Part of the GCL was delineated by drawing a line, using the programmed tool in Adobe Photoshop7.0 (Adobe Systems Inc., San Jose, CA, USA). The total area of the GCL was measured using Object-Image2.15, and the resultant volume (pixels) was converted into micrometers. Individual cells were visualized using the same system described above (10× NA 0.45 objective), and the marker-positive cells were counted in the GCL, SGZ, and hilus. The cells were counted by an observer blinded to the genotype and the treatment status.

Statistical analyses

For every parameter, the values were first calculated separately for each animal before the means and the standard error of the mean (SEM) were determined for the groups. The number of marker-positive cells in a fixed area (cells/mm^2) was converted to the percentage of the number of marker-positive cells in the non-Tg(NS) littermates. Data are expressed as the mean values ± SEM. All statistical analyses were performed with PRISM version 5.0a (GraphPad Software, La Jolla, CA, USA). The data were analyzed by a two-way analysis of variance (ANOVA) between genotypes (non-Tg, L/V-Tg) and treatments (non-stressed, stressed) and with a Bonferroni post hoc test. When an interaction was found, multiple comparisons were performed with the Tukey–Kramer test. Values of $P<0.05$ were considered significant.

Results

Establishment of a chronic intermittent restraint stress model

We first sought to establish an effective restraint tube-based chronic stress model (Supplementary Fig. 1) that causes long-lasting structural changes in the hippocampus. By the protocol with several weeks' continuous restraint stress, it has been pointed out that mice tend to be habituated to the stressor, making it difficult to precisely examine the effects of chronic stress (Kim and Han, 2006). A previous report also indicated that chronic intermittent restraint stress (CIRS) for 2 weeks affected adult neurogenesis in the hippocampus (Rosenbrock et al., 2005). We therefore determined that CIRS is an effective protocol to verify changes in neurogenesis and introduced a resting period during the chronic restraint protocol in which we assess the effectiveness of the stressor using the reduction in body weight gain and the hypertrophy of the adrenal glands as indices.

As a result, our CIRS protocol (Fig. 1) primarily reduced the body growth rate of both non-Tg and L/V-Tg mice under chronic stress (Fig. 2A, B). When the body weight gain, which is expressed as the difference between the end and the beginning of the experiment, was subjected to a two-way ANOVA, we found out a significant effect of treatment ($F_{1,46}=393.98$, $P<0.0001$), but not a genotype effect ($F_{1,46}=1.70$, $P=0.1990$) and no interaction ($F_{1,46}=2.14$, $P=0.1507$) in the short-term experiments. The analysis also revealed a significant effect of treatment ($F_{1,8}=25.66$, $P=0.0010$), but not a genotype effect ($F_{1,8}=0.08$, $P=0.7857$) and no interaction ($F_{1,8}=0.10$, $P=0.7618$) in the long-term experiments. Additionally, the unpaired t-test [non-Tg(ST) vs. L/V-Tg(ST)] revealed that the body weight gain of the L/V-Tg mice (−11.3 ± 0.6%) was significantly reduced compared with that of the non-Tg(ST) animals (−8.6 ± 1.0%) after short-term CIRS (two-tailed, $P=0.0266$; Supplementary Table 1). Although the body growth rate at the resting period was increased in

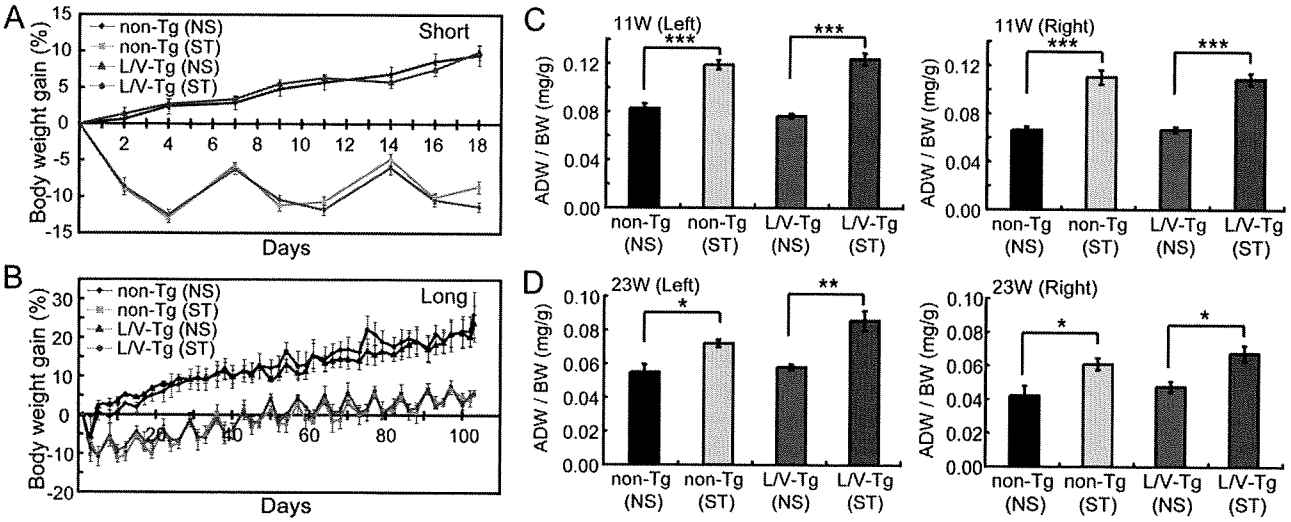

Fig. 2. Chronic intermittent restraint stress (CIRS) induces typical stress symptoms. (A, B) Changes in the body weight gain of mice in the stressed (ST) or non-stressed (NS) groups are plotted; (A) short term; (B) long term. The body weight gain 1 day before perfusion [expressed as the difference between the end and the beginning of the experiment, mean ± standard error of the mean (SEM)] is significantly reduced in stressed animals. (C, D) The left and right adrenal weights after short-term (C) or long-term (D) CIRS are significantly increased in the stressed groups. Data are expressed as the adrenal weight (mg) divided by the body weight (g) (ADW/BW, mean ± SEM). *$P<0.05$, **$P<0.01$, ***$P<0.001$ (Bonferroni, NS vs. ST). Non-Tg, transgenic negative mouse; L/V-Tg, transgenic mouse model of AD with overexpression of an FAD-type PS1; 11W, 11-week-old mice; 23W, 23-week-old mice.

every mouse, the rate of body weight change in the stressed groups showed a distinct fluctuating pattern for 15 weeks compared with that in the non-stressed groups (Fig. 2B). The weight of the right or left adrenal gland was also subjected to a two-way ANOVA, which revealed a significant effect of treatment [11-week-old mice (11W) left, $F_{1,45}=108.26$, $P<0.0001$; 11W right, $F_{1,45}=87.22$, $P<0.0001$; 23-week-old mice (23W) left, $F_{1,8}=28.17$, $P=0.0007$; 23W right, $F_{1,8}=20.57$, $P=0.0019$], but not of genotype effect (11W left, $F_{1,45}=0.24$, $P=0.6301$; 11W right, $F_{1,45}=0.02$, $P=0.8826$; 23W left, $F_{1,8}=4.17$, $P=0.0755$; 23W right, $F_{1,8}=0.57$, $P=0.4714$) and no interaction (11W left, $F_{1,45}=1.72$, $P=0.1963$; 11W right, $F_{1,45}=0.05$, $P=0.8275$; 23W left, $F_{1,8}=1.50$, $P=0.2555$; 23W right, $F_{1,8}=0.00$, $P=1.0000$) (Fig. 2C, D). Finally, the blood corticosterone levels in the groups with short-term chronic stress tended to increase (Supplementary Fig. 3). These results demonstrate that our short-term (3 weeks) and long-term (15 weeks) CIRS protocols can efficiently induce typical physical stress symptoms in mice.

CIRS increases the number of degenerating neurons

Because degenerating neurons appear in L/V-Tg mice without stress after 6 months of age (Chui et al., 1999), the obliteration of neuronal function in the neural circuit involved in cognitive function could be accelerated by the interaction of mutated genes and chronic stress. We thus examined whether stress accelerates neurodegeneration in the L/V-Tg mouse brain by means of the sliver staining: Degenerating neurons were indicated by dense silver precipitates appearing as black grains in their somata (shown by red arrowheads in Fig. 3B) and as cells with numerous fine grains in their somata (shown by red arrowheads in Fig. 3C). On the other hand, typical background signals were indicated by diluted brown particles (shown by a white arrowhead in Fig. 3B). As a result, in L/V-Tg mice degenerating neurons were selectively observed in the circuital areas that correlate with cognitive function. The number of degenerating neurons [% of non-Tg(NS)] was subjected to a two-way ANOVA, which revealed a significant effect of treatment ($F_{1,36}=9.58$, $P=0.0038$), genotype ($F_{1,36}=22.31$, $P<0.0001$), and an interaction ($F_{1,36}=7.18$, $P=0.0110$) in the DG; a significant effect of treatment ($F_{1,28}=8.88$, $P=0.0059$) and genotype ($F_{1,28}=10.13$, $P=0.0036$), but no interaction ($F_{1,28}=1.42$, $P=0.2435$) in the CA3; a significant effect of treatment ($F_{1,32}=25.68$, $P<0.0001$), but not of genotype ($F_{1,32}=2.09$, $P=0.1578$) and interaction ($F_{1,32}=2.19$, $P=0.1487$) in the RCtx; and a significant effect of genotype ($F_{1,27}=8.22$, $P=0.0079$), but not of treatment ($F_{1,27}=1.89$, $P=0.1810$) and interaction ($F_{1,27}=1.07$, $P=0.3108$) in the PCtx (Fig. 3D–G). After short-term CIRS (at 11 weeks of age), the number of degenerating neurons was significantly increased in the DG of L/V-Tg mice [Tukey–Kramer test, $P<0.0001$ vs. non-Tg(NS) and non-Tg(ST); $P<0.001$ vs. L/V-Tg(NS)] (Fig. 3D). The Bonferroni post hoc tests (NS vs. ST) revealed that CIRS increased the number of degenerating neurons in L/V-Tg mice [$P<0.05$, in the CA3 (Fig. 3E); $P<0.001$, in the RCtx (Fig. 3F)]. Especially in the hippocampus of the L/V-Tg(ST) mice, degenerating neurons were drastically increased in the SGZ of the DG, where considerable adult neurogenesis takes place (Fig. 3A). In non-Tg mice, the number of degenerating neurons was slightly increased after short-term CIRS only in the RCtx (Bonferroni test, $P<0.05$, NS vs. ST) (Fig. 3F).

After long-term CIRS (at 23 weeks of age), evidence of neurodegeneration was significantly accumulated in L/V-Tg mice compared with non-Tg mice in various brain regions, including the RCtx and the PCtx (Fig. 4D, E). The number of degenerating neurons was subjected to a two-way ANOVA. This analysis revealed a significant effect of treatment ($F_{1,52}=10.62$, $P=0.0020$), genotype ($F_{1,52}=15.45$, $P=0.0003$), but no interaction ($F_{1,52}=3.38$, $P=0.0719$) in the DG; a significant effect of treatment ($F_{1,44}=7.09$, $P=0.0108$), genotype ($F_{1,44}=19.50$, $P<0.0001$), and an interaction ($F_{1,44}=6.13$, $P=0.0172$) in the CA3; a significant effect of treatment ($F_{1,52}=6.07$,

Fig. 3. The number of degenerating neurons is increased in the brains of stressed animals (short-term). (A) Silver-stained sections of mice exposed to short-term chronic intermittent restraint stress (CIRS) (ST) or left untreated (NS). Scale bar, 100 μm. (B, C) High power pictures of degenerating neurons in the dentate gyrus (DG) (B) and piriform cortex (PCtx) (C) of L/V-Tg(ST) mice (corresponding to the insets in panel A, scale bar, 10 μm). Degenerating neurons are indicated by red arrowheads (B, C); typical background signal is indicated by a white arrowhead (B). (D–G) Graphs indicate the number of degenerating neurons [expressed as % of non-Tg(NS), mean ± SEM] in the DG (D), Cornus Ammonis 3 (CA3) (E), retrosplenial cortex (RCtx) (F), and PCtx (G). Statistical significance; DG [Tukey–Kramer test, ***$P<0.0001$ vs. non-Tg(NS); ###$P<0.0001$ vs. non-Tg(ST); @@$P<0.001$ vs. L/V-Tg (NS)] (D); CA3 (Bonferroni, NS vs. ST, @$P<0.05$) (E); RCtx (Bonferroni, NS vs. ST, #$P<0.05$; @@$P<0.001$) (F). Note that most degenerating neurons in the DG of L/V-Tg(ST) mice are located in the SGZ. Non-Tg, transgenic negative mouse; L/V-Tg, transgenic mouse model of AD with overexpression of an FAD-type PS1; 11W, 11-week-old mice.

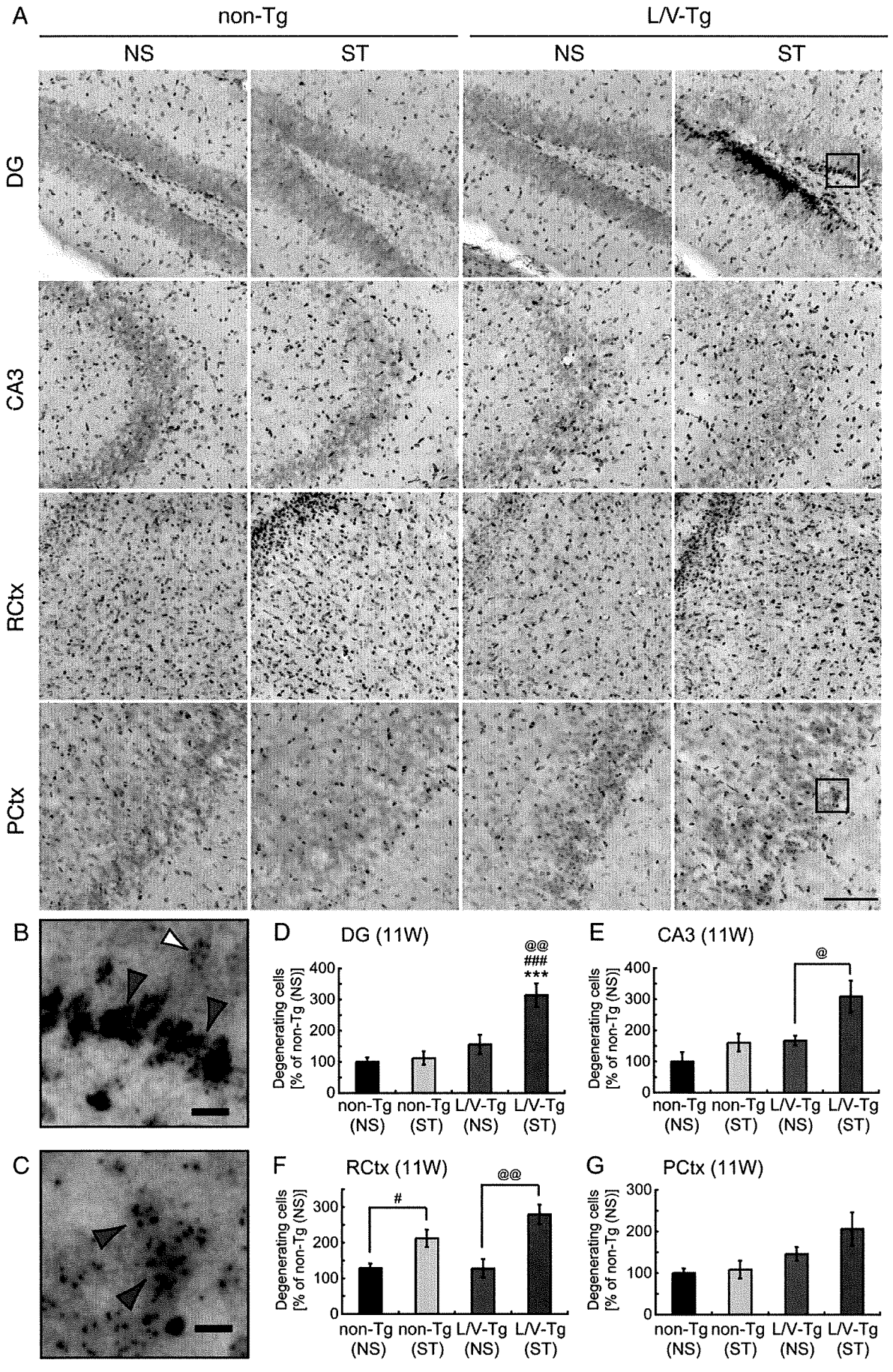
A
non-Tg
L/V-Tg
NS
ST
NS
ST
DG
CA3
RCtx
PCtx
B
C
D
DG (11W)
@@
###
***
Degenerating cells [% of non-Tg (NS)]
400
300
200
100
0
non-Tg (NS)
non-Tg (ST)
L/V-Tg (NS)
L/V-Tg (ST)
E
CA3 (11W)
@
F
RCtx (11W)
#
@@
G
PCtx (11W)